City and Environment Interactions 30 (2026) 100360

Contents lists available at ScienceDirect

City and Environment Interactions

journal homepage: www.sciencedirect.com/journal/city-and-environment-interactions

Research Articles

# Quantifying the co-benefits of a tropical urban park in São Paulo through integrated mobile and stationary monitoring

Jeetendra Sahani [a], Akash Biswal [a], Anubhav Kumar Dwivedi [a], Soheila Khalili [a,b], Hao Sun [a], Maria de Fatima Andrade [c], Giuliano Maselli Locosselli [d], Marco A. Franco [c], Maria Carla Queiroz Diniz de Oliveira [e], Regina Maura de Miranda [e], Leticia Figueiredo Candido [e], Laurence Jones [f], Prashant Kumar [a,b,*]

[a] Global Centre for Clean Air Research (GCARE), School of Engineering, Civil and Environmental Engineering, Faculty of Engineering and Physical Sciences, University of Surrey, Guildford GU2 7XH, the United Kingdom of Great Britain and Northern Ireland
[b] Institute for Sustainability, University of Surrey, Guildford GU2 7XH Surrey, the United Kingdom of Great Britain and Northern Ireland
[c] Institute of Astronomy, Geophysics and Atmospheric Sciences, University of São Paulo, São Paulo, Brazil
[d] Center for Nuclear Energy in Agriculture, University of São Paulo, Piracicaba, Brazil
[e] School of Arts, Sciences and Humanities, University of São Paulo, São Paulo, Brazil
[f] UK Centre for Ecology & Hydrology, Deiniol Road, Bangor LL57 2UW, the United Kingdom of Great Britain and Northern Ireland

ARTICLE INFO

*Keywords:*
Urban Heat
Green Infrastructure
Air Quality
Noise
Tropical Cities
Ecosystem services

ABSTRACT

Rapid urbanisation in tropical megacities intensifies critical environmental stressors, including urban overheating, particulate air pollution ($PM_{2.5}$ and black carbon (BC)), and noise. Green-Blue-Grey Infrastructure (GBGI) offers a promising nature-based solution, yet major knowledge gaps exist regarding its empirical, multifunctional performance and diurnal dynamics in complex tropical settings. This study quantifies how vegetation in a large urban park (Ibirapuera Park, São Paulo) moderates microclimate, improves air quality, and attenuates noise, while assessing the influence of canopy structure and spatial location on these benefits.

A comprehensive mixed-method approach was employed during a 15-day intensive field campaign. High-resolution spatiotemporal data on $PM_{2.5}$, BC, carbon dioxide ($CO_2$), noise, and meteorological parameters were collected through a combination of stationary monitoring at nine ecologically distinct sites and mobile transect monitoring across an urban-park gradient. These observations were complemented by thermal imagery and sky view factor (SVF) analysis.

The park delivered substantial and dynamic environmental benefits. Dense vegetation reduced $PM_{2.5}$ and BC by up to 40%, with mobile gradients of 0.07 and 0.03 μg $m^{-3}$ per 100 m toward the park core, respectively. Cooling averaged 1–2 °C, strengthening to 0.2 °C per 100 m outward in afternoons. A distinct temporal duality emerged: peak cooling occurred in the afternoon, while the strongest air quality improvements occurred in the morning before dense canopy began retaining pollutants. Noise attenuation was modest (~6 dB), with reductions of 0.29 dB and 0.25 dB per 100 m in morning and afternoon transects.

Overall, the park functions as a multifunctional environmental regulator, with benefits shaped by vegetation density, spatial configuration, and time of day. Effective GBGI planning in tropical megacities should prioritise deep vegetative cores (≥250–300 m from major roads), multi-tiered buffers along traffic corridors, and dense canopy structures (SVF < 0.4). Integrating SVF into zoning and expanding networked green corridors can extend these co-benefits, strengthening climate resilience, public health, and urban liveability.

## 1. Introduction

Rapid urbanisation worldwide has intensified environmental challenges, notably urban overheating[1–4]and deteriorating air quality [5–7]. These issues are pronounced in tropical regions due to high solar radiation, anthropogenic emissions, and the properties of built surfaces [8]. The compounded effects lead to exacerbated heat stress and increased morbidity, especially among vulnerable populations[9,10].

* Corresponding author..

https://doi.org/10.1016/j.cacint.2026.100360
Received 9 December 2025; Received in revised form 19 March 2026; Accepted 7 April 2026
Available online 9 April 2026

Air pollutants, including particulate matter with aerodynamic diameters ≤ 2.5 μm ($PM_{2.5}$), nitrogen oxides ($NO_x$), ozone ($O_3$), and black carbon (BC), primarily originate from vehicular emissions, industrial activities, and biomass burning[11,12]. These pollutants interact with urban meteorological processes, forming secondary pollutants that alter radiative forcing and atmospheric stability[13,14], thereby worsening urban living conditions[15,16]. Furthermore, pervasive noise pollution presents an additional environmental stressor[17]. The combined burden of these factors urgently requires multifunctional interventions [18].

Green-Blue-Grey Infrastructure (GBGI) has emerged as a critical nature-based solution. It can enhance urban resilience, improve microclimate, mitigate overheating, improve air quality, reduce noise pollution, and sequester carbon dioxide[2,19,20]. Green infrastructure (e.g., trees, shrubs, green roofs) cools via shade and evapotranspiration [21,22], filters pollutants through deposition and uptake[23–25], and attenuates noise with dense canopies[26,27]. Blue infrastructure (e.g., lakes) complements these effects through evaporative cooling[28,29]. Hybrid grey infrastructure elements, such as permeable pavements and bioswales, enable the ecological performance of green and blue systems. The magnitude of these benefits depends on the type and spatial configuration of GBGI[30,31]. Recent research in Brazil, as summarised in Table 1, has made significant strides in quantifying these benefits. For instance, studies have confirmed that parks can lower particle pollution [32], that canopy cover reduces the Urban Heat Island (UHI) effect[33], and that forest fragments act as barriers for heavy metal deposition[34].

However, a critical synthesis of the literature reveals persistent knowledge gaps, particularly concerning the fine-scale, diurnal dynamics of multiple environmental benefits acting together and their cumulative effects beyond GBGI[4]. Recent global analyses[38] show that tree cooling efficiency varies nonlinearly across climate zones, underscoring the need to examine drivers at multiple scales. As Table 1 illustrates, existing approaches often rely on paired stationary sensors, remote sensing, or single-timeframe sampling. While these methods establish the presence of benefits, they can obscure the continuous spatiotemporal gradients within and away from the urban–park interface. Key unresolved questions include: How do the co-benefits of cooling, air purification, and noise attenuation co-vary spatiotemporally, and to what extent do they exhibit synergistic interactions or trade-offs along gradients from a built-up area to a park core? How do these relationships shift diurnally in response to changing emission patterns, meteorological conditions, and plant physiology? Furthermore, there remains a need to move beyond broad land-cover classifications (e.g., park vs. urban) to understand how vegetation structure (e.g., 3-D canopy analysis through LAI and SVF) and urban morphology drives environmental performance within areas of greenspace [39].

Addressing these gaps requires moving beyond isolated, single–stressor measurements toward integrated, high–resolution monitoring capable of tracking dynamic environmental interactions across continuous spatial gradients. Such an approach is essential to link observed environmental patterns to underlying biophysical drivers and to generate design guidance that extends past generalised park–city contrasts. Building on these identified gaps, this study directly implements an integrated, high-resolution monitoring campaign across the urban-park interface in São Paulo, a tropical megacity. Our methodology simultaneously captures the diurnal cycles of microclimate, air quality, and acoustics along a continuous transect, enabling explicit examination of how multiple benefits co-evolve in space and time in relation to vegetation structure and urban form. This integrated framework allows us to systematically disentangle the drivers of multifunctional environmental services and to quantify the spatial reach and temporal dynamics of these benefits beyond park boundaries.

Our research is guided by two questions: (1) How do structural features of vegetation influence the simultaneous regulation of

**Table 1**
Summary of recent studies on the co-benefits of urban GBGI in tropical environments, emphasising methodological approaches and identifying gaps in high-resolution spatiotemporal analyses of air quality and thermal comfort to contextualise regional research and inform future directions.

| Aim | Study location | Monitoring description (Duration) | Major findings | Reference |
|---|---|---|---|---|
| Compare air quality ($PM_1$, $PM_{2.5}$, $PM_{10}$) and microclimate (temperature, RH, pressure) between vegetated and roadside areas of two urban parks | CIENTEC Park (470 ha large forest) and FSP Park (3 ha small park), São Paulo, Brazil | Park vs. roadside paired stationary low-cost sensor units (PurpleAir Flex); Lidar for vegetation barrier characterisation (Jun 2023 – Apr 2024) | Parks had lower daytime particle levels; FSP showed sharper short-term drops, while CIENTEC sustained low pollution and high humidity. Mitigation varied with vegetation density, barrier porosity, and wind. | Connerton et al. [32] |
| Analyse the role of vegetation in UHI and air pollution mitigation in two Brazilian cities | Urban parks, forest remnants, conservation areas in São Paulo and Curitiba, Brazil. | Remote sensing (Landsat 8 imagery, LST, NDVI and UTFVI indices) + ecosystem service modelling for air pollutant removal (i-Tree Canopy) (Satellite images from 2019) | Higher canopy cover reduced UHI and improved air quality, especially in Curitiba with denser vegetation. | Ribeiro et al. [33] |
| Evaluate the role of forest fragments as barriers against air pollution (heavy metals–Cd, Cu, Pb) | Trianon Parque, Alfredo Volpi Park, Fontes do Ipiranga State Park (PEFI), Carmo Park, São Paulo, Brazil. | Stationary litterfall sampling (edge, middle, core) + Graphite Furnace Atomic Absorption Spectrophotometry (Dry season Jul 2017) | Higher metal deposition near edges and roads, showing the role of forests as pollution barriers. | Ramon et al. [34] |
| Assess tree species tolerance and performance under urban air pollution | 4 biomonitoring zones (MANT, UNNV, PJIC, LAYE), Medellín, Colombia | Field sampling of 54 trees (6 species) + biochemical analysis (ascorbic acid, chlorophyll, pH, RWC) + air quality ($PM_{2.5}$, $PM_{10}$, $NO_2$, $O_3$) monitoring (2014–2019) | *Mangifera indica* was most tolerant, while other species ranged from moderate to sensitive, serving also as bioindicators. | Correa-Ochoa et al. [35] |
| Investigate how climate and air pollution ($PM_{10}$ and airborne metals–Al, Ba, Zn, P), affect *Tipuana tipu* tree growth | Sidewalks and parks, Capuava industrial area, Metropolitan Area, São Paulo, Brazil. | Dendrochronology (tree cores) + bark chemical analysis + satellite LST + $PM_{10}$ and $O_3$ data (CETESB) (tree-ring chronology, 1975–2015; field sampling in 2016) | Air pollution reduced growth more strongly than climate, highlighting the vulnerability of urban trees. | Locosselli et al. [36] |
| Assess thermal comfort and establish comfort thresholds based on microclimate variables and user perception | Zoobotânico Arruda Câmara Park, João Pessoa, Brazil | Microclimate monitoring (RH, wind speed, solar radiation, temperature: air, globe, mean radiant; portable station Davis Vantage Pro2 + globe thermometer) + 900 structured thermal sensation questionnaires (22 days: 12 dry + 10 wet in 2015) | Visitors reported comfort at higher temperatures, with air temperature, radiation, and wind as key drivers, reflecting acclimatisation in hot-humid climates. | Lima et al. [37] |

temperature, pollutant concentrations, and noise levels? (2) At what spatial and temporal scales, do these multifunctional benefits extend into the surrounding urban landscape? The overall objective is to quantify the diurnal spatiotemporal patterns and drivers of multiple environmental benefits provided by GBGI across the urban-park interface in the megacity of São Paulo. This objective is achieved through the following specific aims: 1. To quantify the magnitude and spatial extent of environmental gradients for air quality ($PM_{2.5}$, BC, $CO_2$), microclimate (temperature, humidity), acoustics (noise), and thermal comfort (Physiologically Equivalent Temperature (PET) and Universal Thermal Climate Index (UTCI) indices) along a transect from built-up areas into the core of Ibirapuera Park. 2. To evaluate the role of vegetation

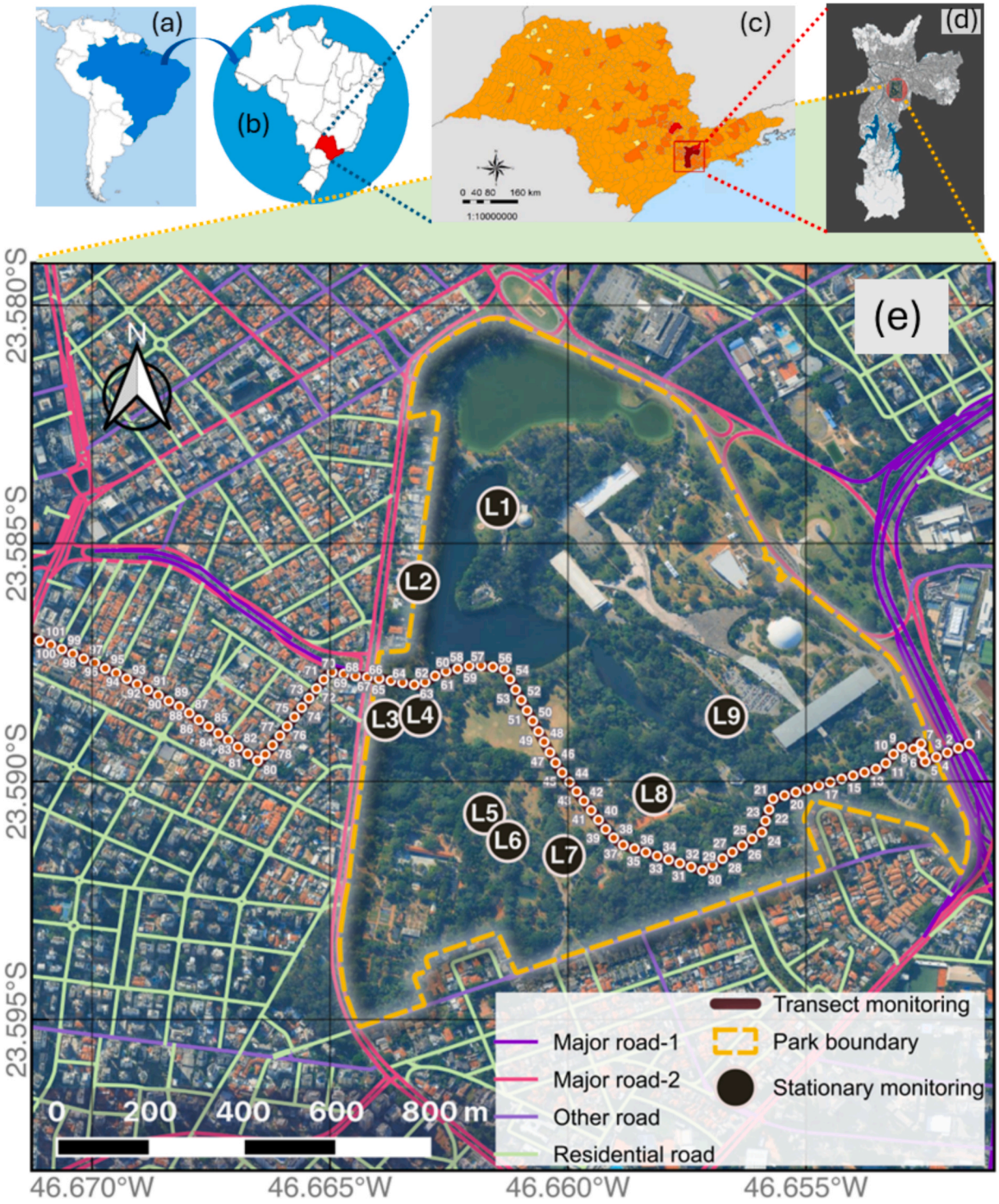


**Fig. 1.** Study site: Ibirapuera Park, São Paulo, Brazil. This figure illustrates the geographical context and monitoring setup for the study: **(a)** Location of Brazil in South America. **(b)** São Paulo State highlighted in red within Brazil. **(c)** São Paulo City outlined in a red box within São Paulo State (shown in orange). **(d)** Ibirapuera Park situated within São Paulo City. **(e)** Detailed layout of Ibirapuera Park showing stationary monitoring locations (L1–9) and mobile monitoring transect (brown line and red dot with white outline) used to assess microclimate, air quality, and noise across and within the park. The transect includes 102 analysis points, spaced at 25-meter intervals on the environmental monitoring transect, covering both park and adjacent urban areas. (For interpretation of the references to colour in this figure legend, the reader is referred to the web version of this article.)

structure and urban morphology, specifically Leaf Area Index (LAI), Sky View Factor (SVF), and proximity to emission sources, in driving the observed patterns of cooling, pollution filtration, and noise attenuation. 3. To assess the diurnal variability and temporal dynamics of these ecosystem services, identifying the key periods of maximum benefit and potential trade-offs (e.g., between cooling and pollutant dispersion) throughout the day. 4. To derive evidence-based recommendations for the strategic design and management of GBGI in tropical megacities that optimise multifunctional benefits for climate resilience and public health.

**Table 2**
Characteristics of nine tree clusters used for stationary monitoring. Each cluster is defined by its location number (L1–9), dominant tree species, representative image, average species height (m), sky view factor (SVF), canopy structure[+], and nearby park features. Tree phenology is indicated as evergreen or deciduous.

| Location number | Cluster tree species | Image | Species height (m) (SVF) | Canopy structure[+] | Nearby features in park | Phenology |
|---|---|---|---|---|---|---|
| L1 | *Libidibia ferrea* (Mart. ex Tul.) L.P. Queiroz |  | 12–17 (0.79) | Round | Lake; Planetarium | Brevi-deciduous |
| L2 | *Tipuana tipu* (Benth.) Kuntze |  | 7–11 (0.55) | Spreading | Lake; Neighbourhood houses; Street | Deciduous |
| L3 | *Caesalpinia pluviosa* DC. |  | 7–9 (0.43) | Spreading | Street; Coffee shop | Deciduous |
| L4 | *Eucalyptus grandis* W. Mill ex Maiden |  | 10–17 (0.41) | Vase | Street; Coffee shop; Lawn | Evergreen |
| L5 | *Pinus elliottii* Engelm. |  | 6–11 (0.49) | Open | City Seedling Nursery; Tennis court; Lawn; Playground | Evergreen |
| L6 | *Centrolobium tomentosum* Guill. ex Benth. |  | 7–12 (0.36) | Irregular | City Seedling Nursery; Tennis court; Lawn; Playground | Deciduous |
| L7 | *Tipuana tipu* (Benth.) Kuntze |  | 8–17 (0.46) | Spreading | Playground; Coffee shops | Deciduous |
| L8 | *Tibouchina granulosa* (Desr.) Cogn. |  | 8–10 (0.85) | Vase | Skatepark; Tennis court; Playground; Pickleball court | Brevi-deciduous |
| L9 | *Araucaria angustifolia* (Bertol.) Kuntze |  | 10–16 (0.37) | Irregular | Lake; Art museum; Afro culture museum; Park | Evergreen |

[+] Source: North SydneyCouncil [42].

## 2. Methodology

### 2.1. Site description

São Paulo, the largest megacity in the Southern Hemisphere, presents a unique context for investigating urban overheating and GBGI performance. Supplementary Information, SI Table S1 presents the summary of São Paulo's weather parameters. Ibirapuera Park, the primary study site (Fig. 1a-e), is a large central 158-hectare park featuring diverse native and non-native tree species, layered vegetation (canopy, subcanopy, understory, ground cover), aquatic elements, and built infrastructure. Opened in 1954, it is São Paulo's most iconic and visited urban park, offering a mix of recreational, cultural, and ecological functions. Bordered by three major traffic-heavy avenues and surrounded by densely built urban areas with limited green connectivity, the site offers an ideal 'living laboratory' for investigating local cooling, air quality, and noise reduction in a tropical city environment[6,40,41].

### 2.2. Study design

This study employed a mixed-method monitoring approach to assess spatiotemporal variation in environmental parameters across a gradient from the core of Ibirapuera Park to surrounding urban areas. Two complementary strategies were implemented: (1) high-temporal-resolution stationary monitoring at fixed sites to evaluate vegetation-induced environmental variations, and (2) high-spatial-resolution mobile transects extending from the park's core to its edges and outward into urban zones, capturing fine-scale spatial and temporal variability across urban–natural gradients.

#### 2.2.1. Stationary monitoring

Stationary monitoring was conducted at nine ecologically representative tree clusters (L1-9, Fig. 1e and Table 2), selected via stratified sampling to achieve variation in canopy architecture, species type (deciduous vs. evergreen), and vegetative density (e.g., LAI). The ecological representativeness of these clusters was first identified using a pre–existing vegetation survey of Ibirapuera Park, which provided spatial information on dominant species group and canopy structures. Final site selection was confirmed through field reconnaissance to ensure that the mapped clusters corresponded accurately to current on–ground conditions. Each site was selected to represent distinct environmental settings, ranging from park interiors to park peripheries adjacent to urban infrastructure. Instruments were placed centrally within shaded tree clusters to reduce solar interference. Observations were repeated across three diurnal windows, morning (07:00–10:00 h), midday (11:00–14:00 h), and afternoon (15:00–18:00 h), to capture fluctuations related to solar zenith, boundary-layer dynamics, and human activity patterns (Section 2.4 and SI Table S2). Each site was monitored for five minutes per session, with measurements taken every 10 s. All sensors were operated synchronously to ensure temporally aligned data collection. To complement stationary monitoring, thermal images were captured at each site using an infrared thermographic camera. Eight images were taken per location, oriented in cardinal and intercardinal directions (N, NE, E, SE, S, SW, W, NW).

#### 2.2.2. Mobile monitoring

Mobile monitoring was performed along a 3 km east–west transect between the Museum of Contemporary Art–University of São Paulo (MAC-USP) pedestrian bridge (east) and Rua Bastos Pereira street (west) (brown path with white outlined red dots in Fig. 1e). This continuous transect (consisting of 102 evenly spaced points at 25 m intervals for analysis consideration) traversed areas of varying vegetative cover, urban infrastructure, and proximity to pollution sources, such as roads and car parks, enabling a detailed comparison between built-up and vegetated environments. The route was walked at a consistent pace of 4.5 km $h^{-1}$ to simulate typical pedestrian exposure conditions while ensuring sensor stability. The environmental parameters were recorded every 10 s, the same as in stationary monitoring, across the three diurnal windows on different days (Section 2.4). GPS data was used to georeference each data point for subsequent spatial analysis and heatmap generation.

### 2.3. Instrumentation

A suite of research-grade portable instruments (SI Table S3) was deployed to monitor meteorological (air temperature ($T_a$), relative humidity (RH), wind speed ($v$), and black globe temperature ($T_g$)), air quality ($CO_2$, $PM_{2.5}$, and BC), and acoustic parameters. Instrument selection was based on validated accuracy, field robustness, and proven performance in peer-reviewed studies[43–45].

Meteorological and $CO_2$ monitoring were conducted using the Testo 400 multifunctional environmental meter (Testo SE and Co. KGaA, Germany), equipped with interchangeable probes: NTC ($T_a$, 0–50 °C), Type K thermocouple ($T_g$, 0–120 °C), humidity probe (RH, 5–95%), hot ball probe (Ø 3 mm $v$, 0–10 m $s^{-1}$), and a wireless $CO_2$ probe (0–10,000 ppm). Air quality monitoring included $PM_{2.5}$ measured with the TSI PDR-1500 photometric aerosol monitor (TSI Inc., USA), operating at 1.7 L $min^{-1}$ with a blue cyclone inlet for sampling and daily calibration using a black inlet. As a photometric instrument, the PDR-1500 estimates particle mass concentrations based on light scattering and may therefore exhibit sensitivity to particle composition, refractive index, and size distribution. The use of a size-selective cyclone inlet and routine field calibration helped ensure consistency of measurements under the prevailing urban aerosol conditions. BC was recorded using the MicroAeth MA200 (AethLabs, USA), an optical aethalometer employing filter-based optical attenuation at 880 nm wavelength with a 0.1 L $min^{-1}$ flow rate and a 17-spot filter cartridge. Filter-based BC measurements can be affected by short-term signal noise and loading artefacts associated with changes in filter attenuation. To minimise these effects, data were processed using the AethLabs Dashboard and the Optimised Noise-reduction Averaging (ONA) algorithm [46], which reduces measurement noise and improves temporal stability of BC estimates under low-concentration ambient conditions. Acoustic conditions were monitored using the RS PRO 1151 sound level meter (RS Pro, UK), configured for A-weighted frequency (dB(A)), fast ("F") response, and active logging mode ("M") within a range of 30 to 110 dB and a resolution of 0.1 dB. Calibration was performed before each session using a 114 dB tone. Geolocation data were recorded using GARMIN ETREX 32X GPS units and the Strava mobile app, providing redundancy and enabling post-hoc spatial analysis [47]. Thermal imaging was conducted using a tablet computer (iPad model A2429, Apple Inc.) with an attachable infrared camera (Flir One Pro, Teledyne FLIR) and a thermal imaging app (FLIR One, version 4.2.0, Teledyne FLIR). All instruments were factory-calibrated and verified *in situ* prior to deployment. Field protocols ensured consistent operation, including gentle handling, regular functionality checks, and standardised transport procedures.

### 2.4. Data collection

Environmental data were collected using a backpack-mounted sensor system (SI Fig. S1) over a 15-day period (13–27 April 2025) (SI Table S2). This window coincided with the transition from late summer to early autumn in São Paulo. The period is marked by favourable atmospheric dispersion (unlike winter inversions), peak vegetation foliation after the rainy season, and the absence of dry–season water stress. These conditions enabled robust evaluation of canopy-driven cooling, air filtration, and noise attenuation under representative tropical meteorology. The monitoring period featured substantial variability in solar radiation, convective activity, and wind regimes—conditions suitable for assessing thermal, air quality, and acoustic dynamics in urban parks[19,48,49]. Mean air temperature was 21.3 °C with 70.1% RH, mostly clear skies (<1% cloud cover), minimal rainfall (0.1 mm

day$^{-1}$), and moderate winds (1.9 m s$^{-1}$) (SI Table S1). These stable yet dynamic conditions provided a suitable baseline for isolating the effects of GBGI structure on diurnal environmental patterns.

Sensor probes were positioned 1.4–1.7 m above ground. To minimise body-induced shading, temperature and radiation sensors were mounted on a rigid 40 cm extension arm, and the backpack was kept partially open for sufficient airflow. The sensor system remained consistently configured throughout the campaign and was positioned behind the operator's direct breathing zone to reduce measurement bias. Self-contamination from resuspended particles was minimised by maintaining a slow, steady walking pace. Repeated passes across the three daily monitoring windows, followed by data averaging, helped reduce short-term disturbances from vehicles, pedestrians, and local particle resuspension. In total, mobile transects were conducted 15 times in the morning and mid-day each, and 16 times in the afternoon, while stationary monitoring occurred 6 times in the morning, 4 times at mid-day, and 5 times in the afternoon. Raw data from all devices were downloaded daily and processed using manufacturer-specific software (e.g., TrakPro™, microAeth® Manager). Across the full campaign, over 180,000 data points were collected, covering $T_g$, $T_a$, RH, $v$, $PM_{2.5}$, $CO_2$, BC, and ambient sound levels. Missing data constituted less than 2.3% of the total dataset, primarily due to occasional GPS signal loss, battery depletion, and sudden rainfall. These gaps were documented and excluded from subsequent analyses to maintain data integrity.

### 2.5. Data analysis

After acquisition, the dataset was structured to support both exploratory and inferential analyses aligned with the study objectives. Spatial and statistical processing enabled interpolation and mapping of environmental parameters across transect and stationary locations. For spatial analysis, the 3 km transect was represented by 102 evenly spaced points at 25 m intervals, extending from the urban edge into the park interior (Fig. 1e). Raw mobile observations were collected every 10 s and georeferenced using GPS, and each observation was assigned to the nearest reference point along the transect for the monitored environmental variables. The data from stationary and mobile monitoring were analysed using python and R.

#### 2.5.1. Mobile data

To quantify the spatial gradients from the park core outward, first-order linear regression models were fitted to the georeferenced mobile data assigned to the 102 reference points along the transect for each environmental parameter. The slope of each regression was used to calculate the mean change per 100-meter distance, with 95% confidence intervals computed to evaluate the statistical robustness of the observed trends. Where repeated mobile observations were linked to the same reference point, these were aggregated prior to regression analysis. To link in-situ observations with landscape features, mobile data were spatially integrated with vegetation structure metrics. The Normalized Difference Vegetation Index (NDVI) was derived from Sentinel-2 satellite imagery using its near-infrared (Band 8) and red (Band 4) reflectance bands.

#### 2.5.2. Stationary data

The analysis of stationary data focused on characterising intra-park variability and diurnal patterns. The analytical treatment included: (i) Site-wise and diurnal averaging: Parameters were averaged by site and by diurnal period (morning, midday, afternoon) to characterise edge-to-core gradients and temporal shifts. (ii) Probability Distribution Function (PDF) analysis: PDFs were employed to evaluate diurnal shifts and identify episodic pollution behaviour beyond what is captured by mean values. (iii) Quantification of vegetation and source Effects: The influence of local environment was quantified by relating measured parameters to canopy structure metrics, specifically SVF and LAI, as well as proximity to emission sources. (iv) Pollution Rose Analysis: Pollution rose diagrams were generated for $PM_{2.5}$ and BC to identify predominant wind directions associated with high pollutant concentrations, thereby assessing the contribution of wind-driven transport from local sources.

#### 2.5.3. Sky view factor (SVF)

SVF is defined as the fraction of the sky hemisphere visible from a point on the ground, with values ranging from 0 (completely obstructed) to 1 (fully open) [50]. It is derived by integrating visible sky angles across the hemisphere, often using fisheye photography[51]. The SVF was derived using a Python script (SI Code S1) to process fisheye images, serving as a key input for thermal comfort evaluation.

#### 2.5.4. Thermal comfort

Thermal comfort was assessed using two indices: the UTCI and the PET, both calculated using Python scripts. PET estimates the equivalent indoor air temperature at which an individual would experience the same thermal sensation as under actual outdoor conditions, assuming identical sweat rate and skin temperature[52]. Its calculation is based on numerical models such as the Munich Energy-balance Model for Individuals and involves simulating the human energy balance and heat exchange processes in outdoor settings. The result is expressed in degrees Celsius (°C); temperatures below 18 °C are considered '*slightly cool*' to '*cold*', 18–23 °C falls within the thermally comfortable range, 23–29 °C is classified as '*slightly warm*', and values above 29 °C indicate increasing thermal discomfort. The UTCI combines air temperature, wind speed, RH and radiation to calculate an indicator of thermal stress experienced by individuals in outdoor settings. Expressed in °C, it is determined through a multi-stage computational process:

$$UTCI = f^{-1}[(T_a, T_m, v_a, RH, M)] \quad (1)$$

where $T_a$ denotes air temperature (°C), $T_m$ represents mean radiant temperature (°C), $v_a$ corresponds to wind speed at 10 m (m s$^{-1}$), RH indicates relative humidity (%), and M stands for metabolic rate (W m$^{-2}$). The UTCI categorises thermal stress into ten categories, ranging from extreme heat stress (above + 46 °C) to extreme cold stress (below −40 °C). The categories in between are very strong heat stress (+38 °C to + 46 °C), strong heat stress (+32 °C to + 38 °C), moderate heat stress (+26 °C to + 32 °C), no thermal stress (+9 °C to + 26 °C), slight cold stress (+9 °C) to 0 °C), moderate cold stress (0 °C to −13 °C), strong cold stress (−13 °C to −27 °C), and very strong cold stress (−27 °C to −40 °C) [53]. In this study, both indices were employed since PET provides an integrated measure of overall thermal perception, while UTCI is more sensitive to short-term variations in meteorological conditions, enabling a comprehensive assessment of thermal stress at the study site[54].

#### 2.5.5. Thermal images processing

Thermal images were analysed to assess surface temperatures of various specimens in the park, particularly the cooling role of GBGI. Dunn's post-hoc test was used for surface temperatures' pairwise statistical comparisons. This method is suitable for identifying significant differences between groups while controlling for multiple comparisons following a non-parametric test.

A custom Python-based model was developed to process thermal images captured during the study period. The aim was to detect and classify visible specimens and estimate the average surface temperature associated with each specimen class (GBGI, Objects, Vehicles, Humans, and Miscellaneous). The images included a visible thermal scale and metadata indicating location, the tree cluster species, and the time of the day. Specimen detection was performed using the YOLOv8 architecture [55,56] through two approaches: (i) a pre-trained model using YOLOv8x weights from the OpenImages dataset, and (ii) a custom-trained model adapted for green and blue infrastructure elements. The latter was trained using 50 manually annotated images via the Roboflow platform, targeting key specimen categories, such as tree, grass, water, and objects. This hybrid strategy enabled the identification of additional

specimen features including humans, vehicles, and structures. The temperature values were derived from the visible thermal scale using Optical Character Recognition (OCR). The region containing the minimum and maximum temperature values was cropped and pre-processed using contrast-limited adaptive histogram equalisation (CLAHE), followed by binarisation and morphological dilation. The cleaned image region was then parsed using pytesseract, a Python tool for OCR, to extract numerical temperature values in °C. A conversion function mapped the grayscale intensity of the detected specimen to the estimated surface temperatures. For each specimen class, the average pixel intensity was computed and translated into a corresponding temperature value, resulting in a structured output linking specimen category and estimated mean temperature. For each processed image, the following were recorded: imageId, capture date and time, location, geographic coordinates, tree cluster species, specimen presence/absence, min/max temperatures from the scale, and the average temperature per detected category.

Statistical analyses were performed in Python using the pandas, NumPy, SciPy, sckiti-posthocs, and statsmodels libraries to assess temperature variability across specimen categories, accounting for factors such as tree species and time of day. The Kruskal-Wallis[57]) test was applied using the kruskal function from scipy.stats package to determine significant differences in temperature distributions among specimen types. For significant results, post-hoc comparisons were conducted using Dunn's test with Bonferroni correction via the scikit-posthocs package[58]. Repeated images were identified through their unique imageID; when duplicates were detected, only one instance was retained for analysis. Finally, to account for the hierarchical data structure and

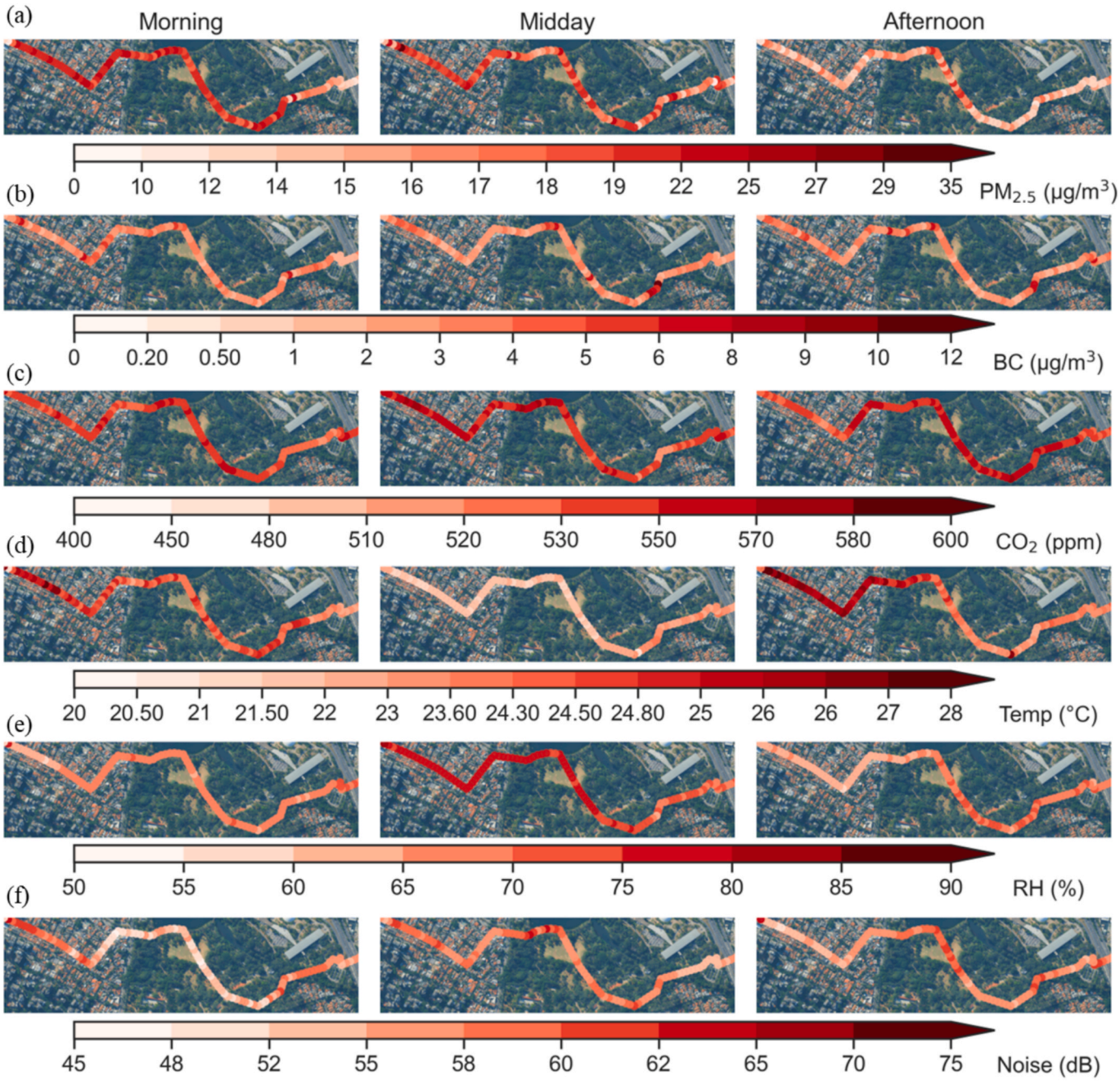


**Fig. 2.** Diurnal spatial patterns of environmental indicators monitored through mobile monitoring, including: **(a)** $PM_{2.5}$, **(b)** BC, **(c)** $CO_2$, **(d)** air temperature, **(e)** RH, and **(f)** ambient noise, along the urban–park transect during morning, midday, and afternoon sessions.

potential interspecific variability, a mixed-effects linear model was fitted using the MixedLM class from the statsmodels library, treating tree species as a random intercept. This model estimated temperature as a function of specimen category and time of day, identifying whether diurnal cycles or specific land-use categories had stronger effects. Estimates and confidence intervals were plotted to assess significance.

## 3. Results

### 3.1. Mobile monitoring

#### 3.1.1. Spatio-temporal patterns

Transect-based mobile monitoring captured fine-scale spatiotemporal environmental gradients (air quality, microclimate, acoustic, and thermal comfort) across the urban–park interface. This high-resolution layout allows for direct comparison between vegetated and non-vegetated zones. Pollutant and microclimate dynamics exhibited strong diurnal cycles. Fig. 2 illustrates spatiotemporal patterns of six environmental parameters along the urban–park transect, highlighting the regulatory influence of vegetation across the eastern roadside, park core, and urban fringe zones. To improve clarity, the results are first described in terms of their general diurnal behaviour across the transect, followed by their spatial gradients from the park core towards the surrounding built-up areas. $PM_{2.5}$ concentrations are typically higher in the morning due to the shallow planetary boundary layer height [59], $CO_2$ reaches its maximum during midday when photosynthetic uptake lags behind anthropogenic emissions [60], air temperature peaks in the afternoon following maximum solar heating[61], and noise levels intensify during high population activity periods.

The peak magnitudes of environmental parameters occurred at different times of day (Fig. 2a-c). For air pollutants, the clearest diurnal contrast was observed in $PM_{2.5}$ and BC, both of which generally showed higher concentrations in the morning and more mixed patterns later in the day. $PM_{2.5}$ peaked at 20.7 $\mu g\ m^{-3}$ in the low-NDVI (SI Fig. S2) urban area west of the park during the morning, dropped to 18.7 $\mu g\ m^{-3}$ within the park, and further declined to 12.8 $\mu g\ m^{-3}$ at the greener eastern roadside. The greatest reduction occurred in the high NDVI areas from dense canopy cover. By afternoon, $PM_{2.5}$ concentrations across all zones fell and became more uniform due to dilution at the mixing boundary layer, ranging between 14.8 and 15.2 $\mu g\ m^{-3}$. In the afternoon, levels inside the park slightly exceeded, by approximately 0.4 $\mu g\ m^{-3}$. This slight difference may be related to reduced air mixing under dense canopy, localised resuspension associated with increased human activity, or hygroscopic particle growth under more humid conditions within the vegetated zone, although these mechanisms were not directly tested in the present study. This indicates that the air-quality benefit of the park was strongest in the morning, whereas later in the day the park interior could become comparable to, or slightly exceed, the urban edges under specific local conditions. Similarly, Abhijith et al. [23] emphasised the pollutant-filtering role of dense tree canopies, supporting the observed reductions in high-NDVI park segments. BC followed a similar spatial gradient in the morning, 3.25, 2.83, and 2.04 $\mu g\ m^{-3}$ from west to east but peaked within the park at midday (3.21 $\mu g\ m^{-3}$), likely due to increased vehicle traffic near the park perimeter during midday, resulting in pollutant advection into the park and limited dispersion under dense canopy cover. BC concentrations are consistent with values found in other locations in São Paulo[62]. By the afternoon, the average BC concentrations within the park declined to 2.97 $\mu g\ m^{-3}$, dropping below the approximately 3.16 $\mu g\ m^{-3}$ observed in adjacent urban areas, indicating a delayed yet effective buffering response. Average $CO_2$ showed subtler variation; concentrations in the park remained stable, rising slightly from 539 ppm in the morning to 549 ppm in the afternoon, likely due to cumulative emissions from visitor respiration, increased soil respiration, and the advection of traffic-related emissions from the park perimeter. In contrast, the western urban zone exceeded 556 ppm at midday due to denser impervious built-up surfaces and limited vegetation. The eastern roadside showed a midday peak followed by an afternoon decline, suggesting localised airflow and street canyon effects.

The urban microclimate varied distinctly across the transect, driven by land cover and vegetation structure (Fig. 2d). The park consistently moderated microclimatic conditions, offering a cooler and more humid environment compared to surrounding urban areas. This cooling effect is closely linked to elevated RH within the park, as denser vegetation enhances both shading and evapotranspiration, which together suppress air temperature while increasing local moisture levels[38,63]. In terms of diurnal behaviour, the strongest thermal contrast emerged during midday and afternoon, when the park retained cooler and moister conditions than the surrounding built-up areas. At midday, air temperatures within the park were 1 to 2 °C lower than in adjacent zones, with a recorded minimum of 22.4 °C attributed to dense canopy shading and evapotranspiration. In the morning, the air temperature peaked in the western urban zone at 24.8 °C, dropped slightly within the park (24.2 °C), and reached the lowest value (22.7 °C) at the exposed eastern roadside. These patterns support earlier findings by Bowler et al. [21] and Gago et al. [22], who demonstrated the cooling effects of urban green infrastructure through shading and evapotranspiration. By afternoon, heat accumulated in the urban western zone (25.8 °C), whereas the park remained cooler at 23.9 °C. RH showed complementary patterns (Fig. 2e). Morning RH ranged from 66.1% (west) to 70.4% (east), rising at midday to 73.1% in the park, driven by transpiration. Although the eastern roadside peaked at 76.3%, it dropped sharply to 63.3% by afternoon, unlike the park, which sustained 68.4%. These inverse gradients in temperature and RH suggest strong vegetation-driven regulation, where cooler, moist conditions reinforcing each other within the park core. This underscores the park's buffering role, particularly during periods of peak solar radiation, consistent with Gunawardena et al. [28], who reported higher humidity in vegetated areas due to active transpiration and microclimate regulation.

Fig. 2f shows that the noise levels increased from a morning range of 54.5–55.7 dB to midday peaks, with the urban western area reaching 58.1 dB, the park reaching 57.3 dB, and the eastern edge reaching 55.4 dB. In the afternoon, noise level reached up to 58.7 dB near Av. Pedro Álvares Cabra highway, however, some of the highest noise peaks appeared within the park itself, possibly reflecting localised activities or internal sources. The co-location of high NDVI and lower midday noise levels highlights vegetation's potential role in acoustic buffering, consistent with findings by Grote et al. [27] and Stuhlmacher et al. [64], who noted that dense canopies can mitigate urban noise via sound absorption and deflection.

Having outlined the general diurnal behaviour of the main variables, Fig. 3 further quantifies how these environmental conditions changed spatially from the park core (high NDVI Point 34, Fig. 1e) towards the surrounding built-up areas. A first-order polynomial fit (Fig. 3) was applied to quantify spatial gradients in environmental variables across the transect. This approach captures dominant monotonic trends while maintaining comparability and minimising overfitting, with 95% confidence intervals reflecting temporal variability. SI Table S4 summarises the corresponding correlation coefficients (r) and p-values, and gradients that were not statistically significant were interpreted cautiously as indicative spatial tendencies rather than robust statistical relationships. Accordingly, the discussion below focuses on statistically supported gradients, while non-significant patterns are described in more tentative terms where relevant [65,66]. For air quality, $PM_{2.5}$ levels gradually rose away from the park, particularly in the morning, with an increase of approximately 0.07 $\mu g\ m^{-3}$ per 100 m away from the park boundary and into the surrounding urban area. These concentrations remained lowest near Point 34, where dense canopy likely enhanced pollutant filtration. BC followed a similar trend in the morning and afternoon, rising by up to 0.04 $\mu g\ m^{-3}$ per 100 m across the gradient. Interestingly, midday BC levels showed a slight decrease toward built-up areas, possibly due to temporary trapping under dense foliage, supporting

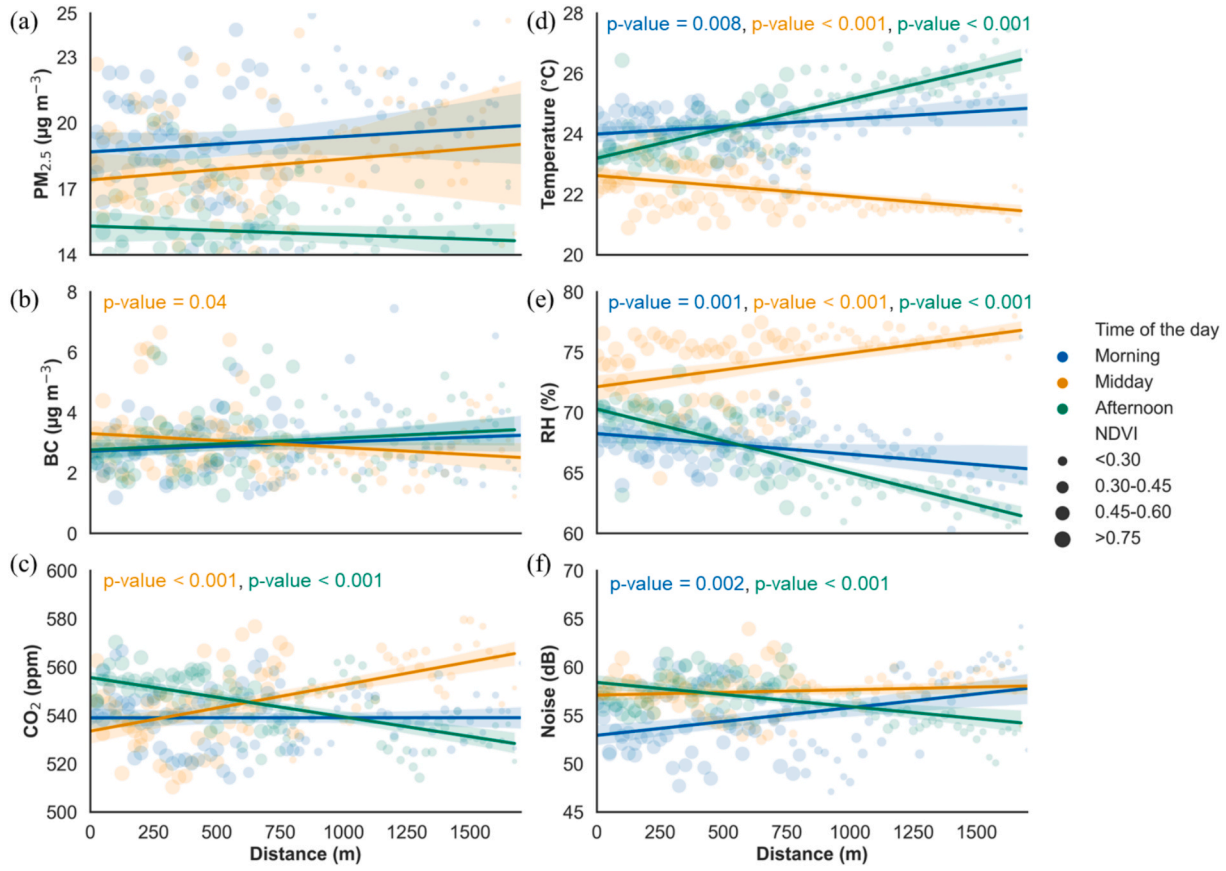


**Fig. 3.** Spatial gradients of environmental parameters along the measurement transect from the park core (Point 34), across the park boundary (~750 m), and into the adjacent built-up environment. Each point represents a mobile observation, where the marker size qualitatively reflects local NDVI and the colour denotes the time of day following the legend scheme (morning, midday, afternoon). Regression lines shown in each panel are first-order (linear) polynomial fits, and the shaded envelopes represent 95% confidence intervals of the modelled trend. Significant regression trends are annotated with in-panel coloured p-value labels, where the text colour directly corresponds to the same time-of-day colour scheme used in the legend. Panels present spatial variation of: (a) $PM_{2.5}$, (b) black carbon (BC), (c) $CO_2$, (d) air temperature (°C), (e) relative humidity (RH %), and (f) noise level (dB).

observations of localised canopy effects [25]. $CO_2$ demonstrated the strongest spatial variation among all variables: during midday, it increased by nearly 2 ppm per 100 m outward from the park. This was followed by a sharp afternoon decline, as levels dropped by more than 1.6 ppm per 100 m, likely aided by vegetation-driven uptake and improved vertical air mixing. Microclimate gradients showed a similarly coherent pattern. Morning temperatures rose slightly from the park outward (0.05 °C per 100 m), and this gradient steepened in the afternoon, reaching almost 0.2 °C per 100 m. RH displayed an inverse relationship, decreasing progressively toward low-NDVI zones, with the most significant drop occurring in the afternoon (about 0.53% per 100 m), an effect also noted in Zölch et al. [29]. Noise levels exhibited a modest spatial gradient across the transect. In the morning, values decreased by approximately 0.29 dB per 100 m from the built-up zone to the park core, suggesting attenuation effects from vegetation. This pattern reversed in the afternoon, with noise rising by 0.25 dB per 100 m toward the highway, indicating shifting noise sources and reduced buffering at the urban edge.

### 3.1.2. *Thermal comfort along the transect*

In addition to individual parameter analysis, the data also support thermal comfort evaluation, offering a comprehensive understanding of how urban green spaces buffer environmental stressors and enhance outdoor comfort. Thermal comfort along the mobile transect exhibited pronounced diurnal and spatial variability, with both PET and UTCI indices indicating variable thermal comfort patterns between the park and built-up area, with improvements evident mainly in the afternoon (Fig. 4a-b, SI Table S5). In the morning, thermal stress levels were relatively mild across both environments, with mean PET values of 19.5 °C in the built-up area and 19.3 °C in the park, and UTCI values of 22.2 °C and 22.0 °C, respectively. By midday, thermal stress notably intensified in both environments, with slightly lower mean PET (24.3 °C) and UTCI (26.6 °C) values in the park compared to the built-up area (PET: 24.8 °C; UTCI: 27.0 °C). However, median values suggest the opposite trend, with the park showing marginally higher thermal stress (PET: 24.5 °C vs 23.0 °C; UTCI: 27.1 °C vs 25.0 °C). This midday pattern reflects the influence of higher relative humidity in the park, which can offset its air temperature advantage and increase heat stress. Although comfort improved in the afternoon, built-up areas remained warmer (PET: 22.0 °C; UTCI: 24.4 °C) than the park area (PET: 20.7 °C; UTCI: 23.3 °C). The built-up area also showed broader variability and higher maximum values, reflecting greater heat retention and slower cooling. These observations are broadly consistent with recent findings highlighting how integrated urban greenery can effectively reduce thermal stress across urban contexts[67–69]but suggest that the effects vary with time of day.

Both PET and UTCI showed a clear spatial gradient, with the highest values at the eastern end near the highway and car park, reflecting the warming effect of impervious surfaces and traffic, as reported in urban heat island (UHI) studies[70]. Values declined steadily into the park's vegetated core, highlighting the cooling influence of trees and greenery [38,71], though a local increase occurred in an open grassland area lacking tree cover. In the western built-up area, thermal comfort values were comparable to within parts of the park, due to buildings shading,

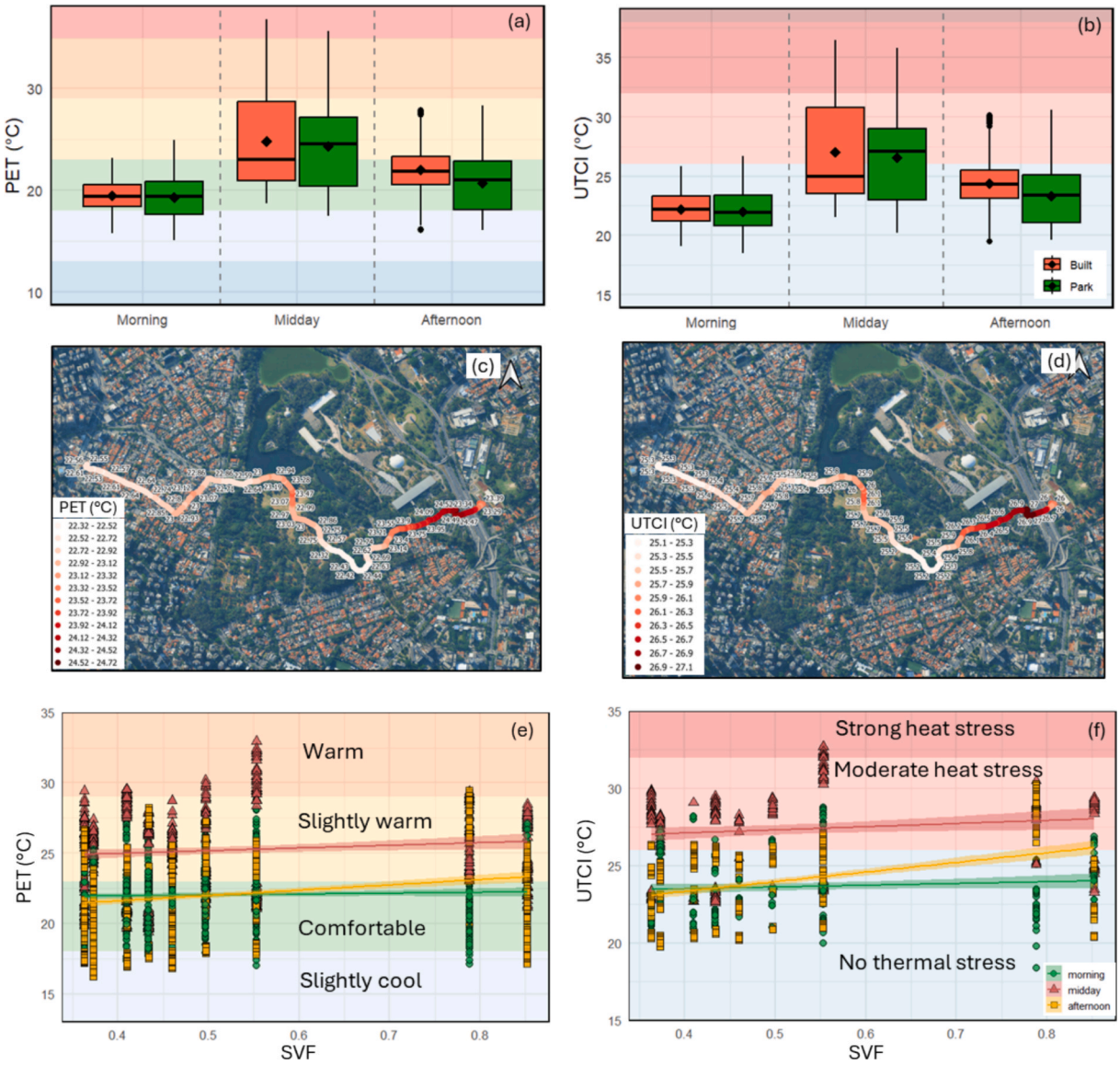


**Fig. 4.** Thermal comfort analysis along the mobile monitoring transect using the PET and UTCI indices. (a) Boxplots of PET values in the built-up area and park during morning, midday, and afternoon. (b) Boxplots of UTCI values in the built-up area and park during morning, midday, and afternoon. (c) Spatial distribution of PET along the transect from built-up area to park during afternoon on a representative day (16th April 2025). (d) Spatial distribution of UTCI along the transect from built-up area to park on a representative day (16th April 2025). (e) PET values plotted against SVF for morning, midday, and afternoon. (f) UTCI values plotted against SVF for morning, midday, and afternoon. PET and UTCI thermal comfort categories are shown as background colour bands.

reduced solar exposure, and urban geometry, despite relatively low tree density, consistent with research showing that shading can reduce thermal stress [72]. The maps in Fig. 4c–d show a representative monitoring day afternoon values, with PET ranging from 21.2 to 24.5 °C and UTCI from 23.9 to 27 °C, capturing the spatial contrasts between built-up and park area.

The relationship between SVF and thermal comfort conditions revealed consistent patterns across the day, with higher sky exposure generally associated with increased thermal stress (Fig. 4e-f). Linear regression confirmed that PET increased with SVF throughout the day, with morning and midday relationships significant ($p < 0.05$; slopes = 5.14 and 4.06, respectively) and the afternoon relationship highly significant ($p < 0.001$; slope = 10.6). For UTCI, the relationship was significant in the morning ($p < 0.05$; slope = 6.06) and afternoon ($p < 0.01$; slope = 8.77), but not significant at midday ($p > 0.05$). These results suggest that canopy cover (low SVF) plays a key role in improving thermal comfort in the afternoon, whereas its effect is minimal in the morning. The weaker midday relationship likely reflects the saturation of thermal stress under peak solar radiation, where SVF alone becomes a less dominant factor, consistent with previous studies showing that during daytime other climatic variables and urban features modulate thermal comfort conditions (e.g., southern Brazil; [73]). Interaction models further indicated that the effect of SVF on both PET and UTCI was significantly stronger in the afternoon than in the morning. Fig. 4e-f illustrate that areas with higher sky exposure experienced higher thermal stress, particularly during midday and afternoon periods, whereas shaded or lower-SVF areas corresponded to comparatively cooler conditions, highlighting the mitigating role of urban shading and vegetation on thermal comfort. These results are in line with previous studies showing that higher SVF increases thermal stress [74], while shading and vegetation mitigate heat and improve thermal comfort conditions [75], although the magnitude of this effect may vary temporally and across different locations[76,77].

### 3.2. Stationary monitoring

#### 3.2.1. Canopy structure influence on edge-to-core gradients

Boxplots analysis (Fig. 5) and summary statistics of environmental parameters (SI Table S6) showed clear differences among the stationary sites, influenced by both traffic proximity and canopy structure. $PM_{2.5}$ and BC were highest at road-proximal edges L1 and L2 (~23.3 and ~ 2.7 μg $m^{-3}$ respectively) and ~ 31–40% lower in the vegetated core (L5–L6), consistent with distance-decay from sources [78,79]and enhanced deposition/dispersion within denser canopies[80,81]. Wider distributions at peripheral sites (e.g., L1–L3, L9) indicate episodic pollution from traffic, while tighter interquartile ranges in the interior reflect stable conditions.

These patterns align with general canopy architecture differences between the park's edge and core. The interior areas are characterised by high stand density and multi-layered, irregular crowns that increase aerodynamic roughness and filtration potential[82]. In contrast, edge sites often feature more open or vase-shaped canopies, providing less structural resistance to pollutant influx. It is important to note that this analysis identifies associations between observed canopy structure and environmental benefits; it does not isolate the effects of species from confounding factors such as stand density, tree height, and local microclimate, which were not independently quantified. $CO_2$ varied little among sites but was ~ 5–7% lower at interior locations, consistent with enhanced photosynthetic uptake and reduced anthropogenic emissions. Microclimate responses were concordant: edge sites were ~ 2.5 °C warmer, while RH was 4–6% higher in the cooler shaded interiors. Noise levels declined from entrances (~58.5 dB) to the core (~52 dB), indicating acoustic shielding by vegetation [83,84].

#### 3.2.2. Diurnal variability

PDFs were analysed for morning (07:00–10:00 h), midday (11:00–14:00 h), and afternoon (15:00–18:00 h) periods (Fig. 6). $PM_{2.5}$ distributions were narrowest in the morning, broadened and shifted upward at midday with a long tail to 40–45 μg $m^{-3}$, and contracted slightly in the afternoon. This pattern likely reflects the combined influence of advected traffic-related plumes and enhanced photochemical activity that can promote secondary aerosol formation during periods of stronger solar radiation and atmospheric mixing. This is consistent with a combination of plume advection from traffic, potential secondary formation[85,86]. Particle resuspension may represent an additional contributing mechanism; however, in the absence of direct corroborating indicators such as coarse particle fractions or wind-speed relationships, this interpretation is treated here as a plausible hypothesis rather than a confirmed process. This hypothesis is supported by two contextual observations. First, the highest concentrations and longest distribution tails occurred at open-canopy edge sites (e.g., L1, L2, L9), which are directly exposed to roadway emissions and mechanical turbulence generated by vehicle movements and pedestrian activity on paved surfaces, both known drivers of resuspension [23]. Second, the peak in distribution breadth coincided with midday period, when convective turbulence and human activity within the park are typically enhanced, creating ideal conditions for lifting settled particles back into the near-surface atmosphere. Although direct supporting indicators (e.g., $PM_{10}$ fractions or wind-speed correlations) were not examined in this study, the spatial exposure gradient and diurnal timing observed here are consistent with resuspension-related processes reported in urban environments. BC PDFs were right-skewed across all periods, with the heaviest tails at edge locations, consistent with traffic emissions [79,87]. Denser interior canopies effectively dampened these extremes, reflecting the buffering influence of vegetation on pollutant dispersion and mixing. $CO_2$ PDFs exhibited weak bimodality. Morning levels were higher due to respiration, narrowing and shifting downward by midday due to photosynthetic drawdown and ventilation [60,88]. An afternoon

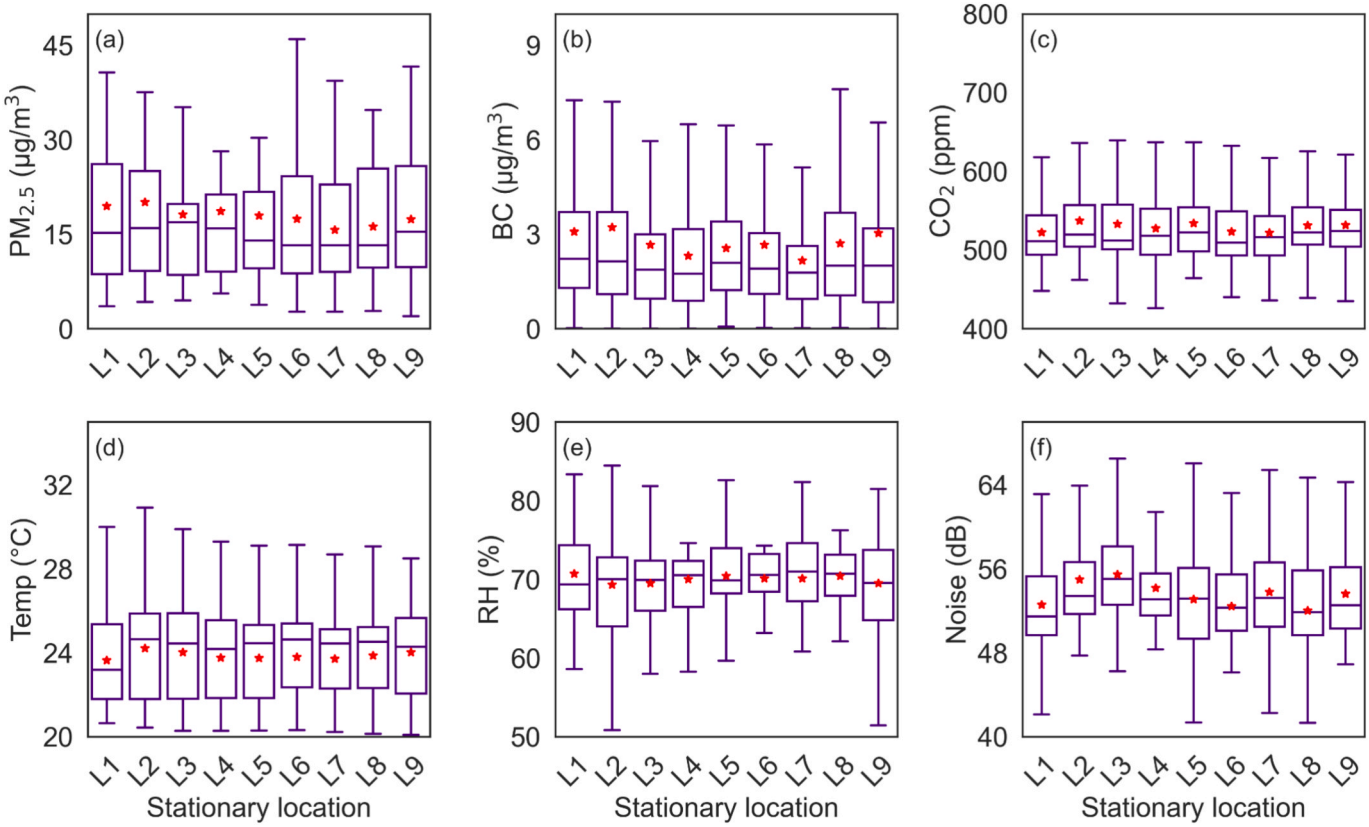


**Fig. 5.** Boxplots of $PM_{2.5}$, BC, $CO_2$, temperature, RH and noise levels across nine stationary sites in Ibirapuera Park. Red stars indicate mean values. (For interpretation of the references to colour in this figure legend, the reader is referred to the web version of this article.)

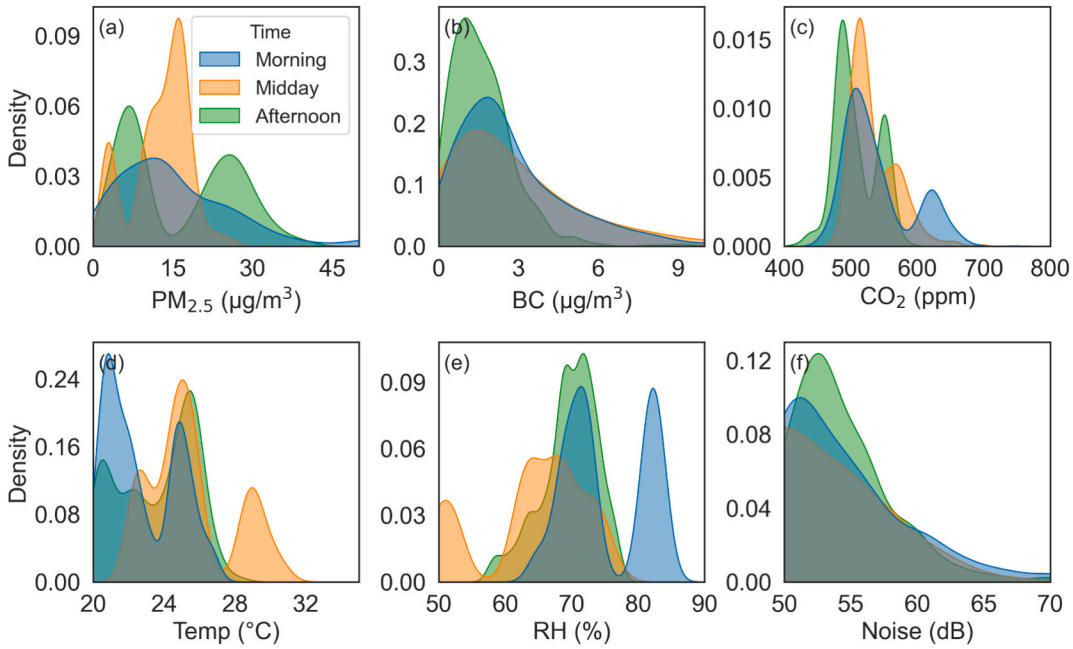


**Fig. 6.** Probability Density Functions of PMBC, temperature, RH, $CO_2$, and noise levels by time of day (morning, mid-day, afternoon). Afternoon peaks and afternoon declines illustrate diurnal trends and the temporal influence of GBGI on environmental conditions.

secondary mode likely reflects advective inputs. Temperature distributions tracked solar radiation, shifting rightward and broadening at midday. RH showed an inverse, complementary pattern. Vegetation moderated extremes through shading and transpiration[89]. Noise PDFs showed a clear diurnal progression, with levels rising from morning to afternoon due to increased recreational activity. Interior zones maintained lower, more stable noise levels due to acoustic shielding[83,84].

### 3.2.3. *Integrated analysis: Source proximity, wind, and vegetation as governing factors*

Pollution rose diagrams for $PM_{2.5}$ (Fig. 7) covering only the period of monitoring, showed the highest concentrations were associated with NW and W winds. Sites closest to source vectors (e.g., L3: 84 m to road) experienced frequent high-concentration episodes. In contrast, interior sites farther from roads and closer to footpaths (e.g., L5) showed reduced pollutant inflow. Integrating spatial and temporal signals demonstrates that environmental quality is collectively shaped by proximity to emission sources, vegetation structure, and wind direction[23,80]. Directional rose plots of BC (µg $m^{-3}$) across nine stationary sites (L1–L9) reveal wind-driven transport patterns and spatial variability in pollution exposure. In Fig. 8, the BC rose plots for sites L1–L9 show that edge locations generally exhibited stronger directional BC signatures than interior locations. This pattern indicates a more direct influence of traffic-derived combustion plumes at roadside sites, whereas the weaker and less distinct directional signals at interior sites are consistent with attenuation during transport through the vegetated park interior. The largest benefits in cooling, pollutant removal, and noise attenuation were consistently observed at mid-park sites (L4–L6), underscoring the value of interior zones with high vegetation density and structural complexity [82].

### 3.2.4. *Spatial and diurnal variability in thermal comfort*

Thermal comfort, quantified by UTCI and PET indices, showed marked spatial and diurnal variability (Fig. 9.a-b). Midday periods consistently induced the highest thermal stress (e.g., UTCI: 24.35 °C at L4 to 29.32 °C at L2). A clear association was found with SVFs, locations with high SVF (e.g., L8: 0.85) reported higher UTCI and PET values, while those with low SVF (e.g., L6: 0.36) maintained lower, more comfortable values throughout the day. This pattern is strongly linked to the degree of canopy closure and surrounding site conditions (Table 2). Stations with low SVF, typically associated with dense, multi-layered vegetation, buffered radiant heat gain and reduced thermal exposure even at midday. In contrast, locations with higher SVF, characterised by more open or vase-shaped canopy structures, allowed greater solar penetration, leading to higher UTCI/PET. Local context further reinforced these trends: clusters adjacent to paved or recreational surfaces (skatepark, tennis courts at L8) exhibited stronger heat stress, while lakeside locations (L1, L9) benefited from moderated conditions. Together, these results highlight how canopy coverage (as measured by SVF) is a primary driver of microclimatic comfort in urban parks, with local land use providing additional modulation.

## 3.3. *Surface temperature variation across specimen categories and tree species*

Surface temperatures from thermal imagery collected during the campaign from each of the nine stationary tree cluster locations were extracted, averaged, and reclassified into specimen categories and tree species. SI Table S7 presents average minimum and maximum surface temperatures (°C) by tree species. Table 3 compares daily mean surface temperatures across five categories (GBGI, Objects, Vehicles, Humans, Miscellaneous) using thermal imagery collected on seven monitoring dates in April 2025. Day 4 recorded the highest average temperature, while Day 6 and 7 were the coolest. GBGI consistently exhibited the lowest mean temperature (17.25 °C), confirming its cooling effect. Objects and Humans showed higher averages (~18–19 °C), while Vehicles had intermediate values with greater day-to-day variability. To determine whether surface temperatures differed significantly between specific specimen categories, pairwise statistical comparisons were performed for all category combinations, and adjusted p-values were reported (SI Table S8). Dunn's post-hoc test with Bonferroni correction was used, following a Kruskal-Wallis test due to non-normal data distribution. GBGI had significantly lower temperatures than Humans ($p < 0.001$) and Vehicles ($p = 0.001$), reinforcing its thermal moderation role. Humans also differed from Miscellaneous ($p < 0.05$). No other comparisons were significant.

Fig. 10a illustrates the distribution of surface temperatures across categories during morning, midday, and afternoon periods. The density

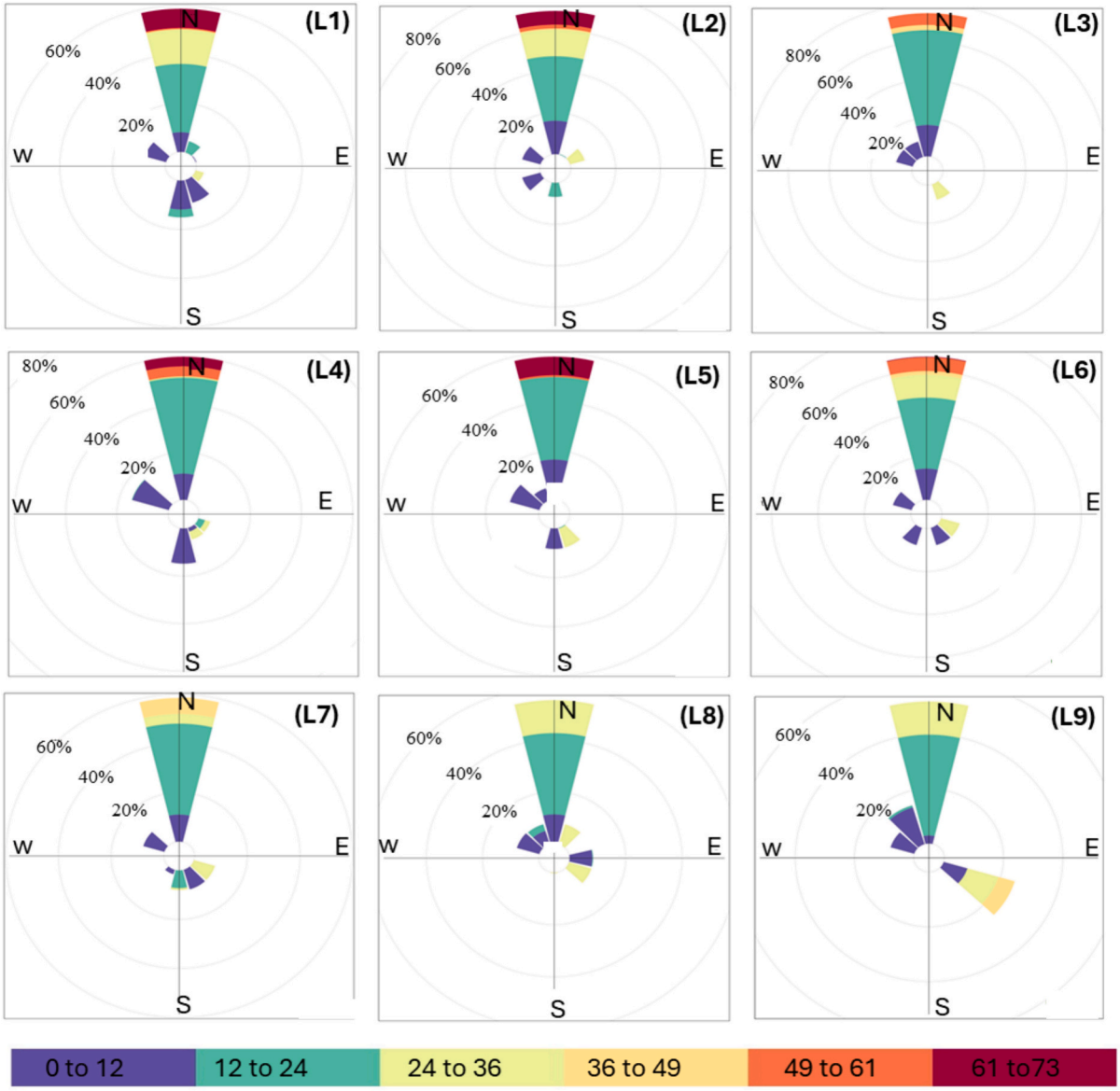


**Fig. 7.** Pollution rose diagrams of $PM_{2.5}$ at the nine stationary locations (L1–L9) in Ibirapuera Park, showing concentration frequency by wind direction. Elevated $PM_{2.5}$ levels are linked to north-westerly (NW) and westerly (W) winds near major roads (e.g., L1, L3, L9), while interior sites (e.g., L5, L6) show lower, less directional concentrations, indicating effective vegetative buffering.

curves reveal a consistent diurnal pattern across most categories: morning distributions were shifted toward higher values, while afternoon distributions clustered toward lower values. Kernel density curves for all image categories (Fig. 10b) further delineate the thermal performance of each group. GBGI exhibited a notably narrower and cooler distribution, peaking around 17 °C, which reinforces its primary role in thermal mitigation. In contrast, 'Objects' and 'Vehicles' exhibited broader ranges and higher average temperatures, indicating greater heat absorption and variability, a pattern consistent with findings of elevated thermal loads in built-up areas[32]. The 'Humans' category displayed a right-shifted distribution with values above 19 °C. Overall, these findings align with the established understanding that vegetated surfaces maintain lower temperatures than built materials[33], while also capturing the distinct diurnal warming and cooling cycles of different surface types.

Fig. 10c and SI Table S9 show model coefficients with 95% confidence intervals, comparing categories to GBGI and time of day to the afternoon baseline. GBGI during the afternoon was used as the reference category, as it represents the most moderated condition against which other effects were compared. The intercept (17.21 °C) therefore corresponds to the average temperature of GBGI in the afternoon. Morning temperatures were significantly higher than afternoon values ($\beta = 1.36$, $p < 0.001$), while midday temperatures showed no significant difference (Fig. 10c). Vehicles exhibited a non-significant trend toward higher temperatures relative to GBGI ($\beta = 1.01$, $p = 0.089$). These patterns reflect diurnal microclimatic shifts, where morning heat accumulation is greater in exposed areas. The violin (Fig. 10a) plots confirmed these model outcomes (SI Table S9).

Fig. 11 shows the average minimum and maximum surface temperature values for each monitored tree cluster location to highlight species-specific thermal performance. *Pinus elliotti* and *Centrolobium tomentosum* had the lowest maximum temperatures (12.2–20.6 °C), reinforcing their cooling efficiency, while *Araucaria angustifolia* exhibited the higher values (22.1 °C), and *Libidibia ferrea* (C. Ferrea) exhibited the highest minimum (14.9 °C), pointing to reduced cooling efficiency. This species-specific performance is likely linked to canopy architecture and physiology, where dense canopies enhance shading and reduce radiant heat. The thermal imagery confirms that vegetation structure

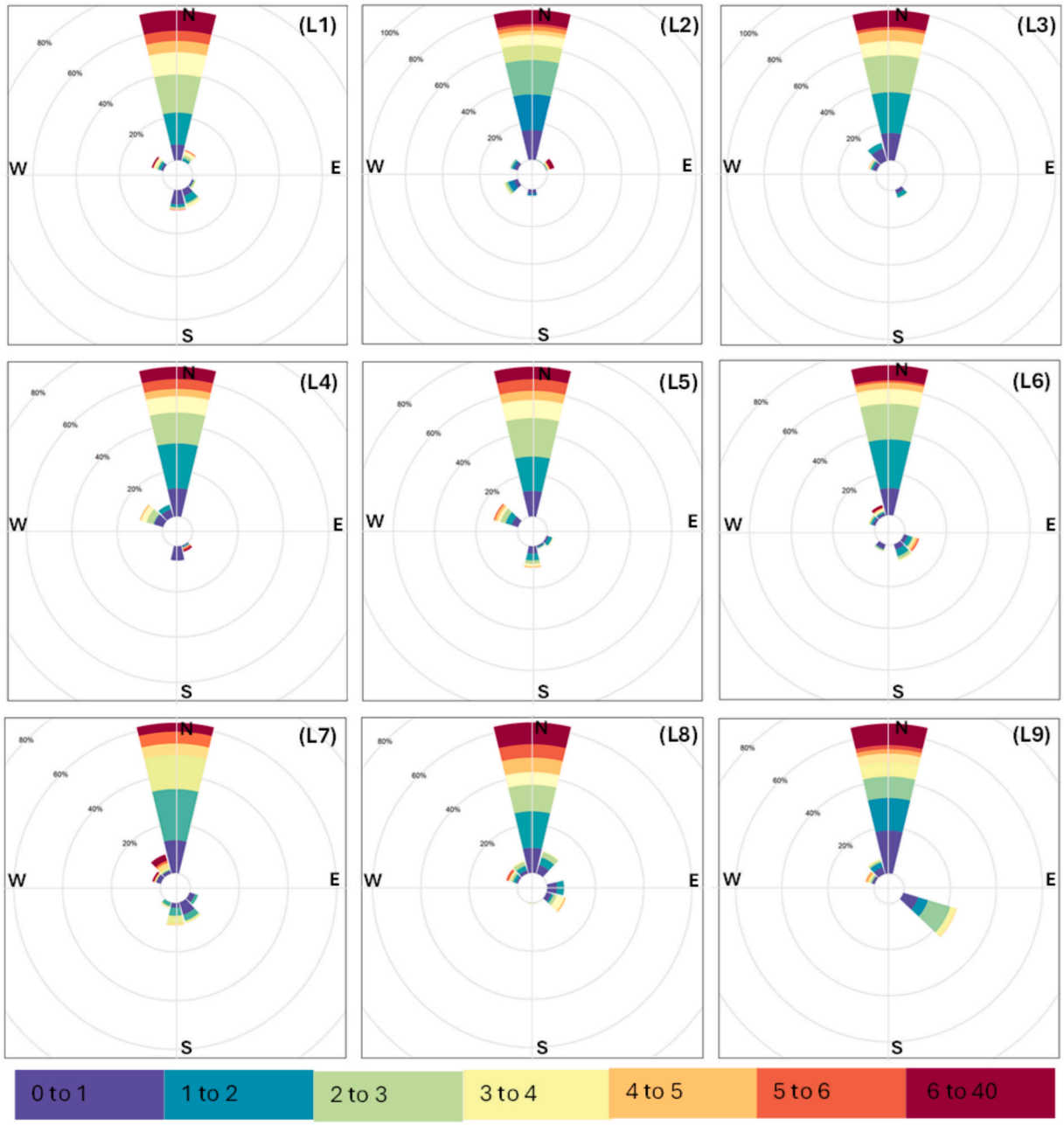


**Fig. 8.** Pollution rose diagrams of BC at the nine stationary locations (L1–L9) in Ibirapuera Park, showing concentration frequency by wind direction.

and species selection are primary drivers of surface temperature regulation. Shaded areas beneath specific tree species exhibited markedly lower temperatures than unshaded areas. The cooling effects extended beyond park boundaries, particularly during peak afternoon hours, indicating GBGI's significant potential to alleviate surrounding urban heat. Collectively, these results reinforce the critical role of green infrastructure in shaping urban microclimates across spatial and temporal scales, with strong implications for climate adaptation and public health.

## 4. Discussion

### 4.1. Air pollution dynamics

The spatiotemporal patterns of $PM_{2.5}$ and BC across the urban-park transect reveal a complex relationship between vegetation and air quality that extends beyond simple filtration. While the observed morning reduction in $PM_{2.5}$ within high-NDVI areas aligns with established understanding of vegetation as a pollution filter, the afternoon elevation of $PM_{2.5}$ within the park relative to urban edges highlights a more nuanced interaction. This phenomenon can potentially be understood through the dual role that dense vegetation plays in both removing pollutants and modifying local microclimate in ways that may elevate concentrations.

The consistent morning reduction in both $PM_{2.5}$ and BC within the park core demonstrates the well-documented filtration capacity of dense canopy cover [28]. As previous research has indicated, vegetation functions as a natural air filter, with tree canopies intercepting particulate matter through surface deposition[90]. However, the afternoon elevation of $PM_{2.5}$ within the park, coupled with the midday BC peak, suggests that the same vegetation that filters pollutants may also inhibit their dispersion. The dense canopy cover that facilitates filtration during

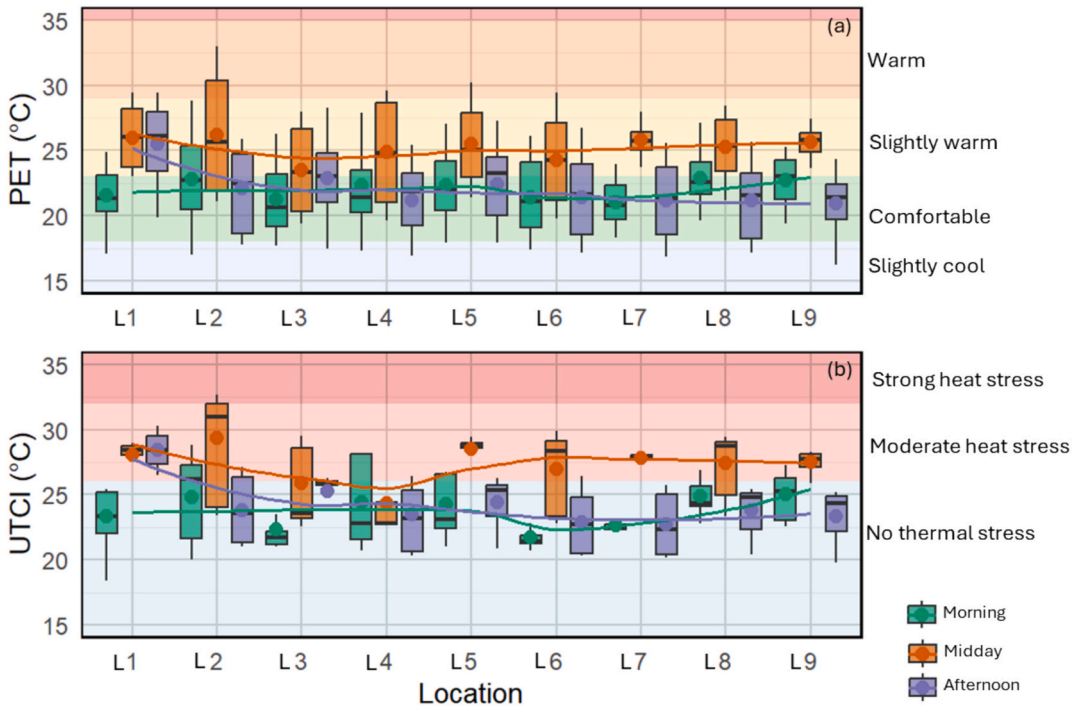


**Fig. 9.** Boxplots of thermal comfort indices across nine stationary monitoring locations during morning, midday, and afternoon periods. (a) PET distribution, and (b) UTCI distribution. Shaded background bands represent standard thermal stress categories. Non-linear trendlines connect the mean values across locations for each time of day, highlighting diurnal variations in thermal comfort.

**Table 3**
Average surface temperature with ± standard deviations (°C) by specimen category (GBGI, Objects, Vehicles, Humans, Miscellaneous) across seven monitoring days in April 2025, followed by an overall mean. Missing data are indicated with a dash (–). Ambient temperature values represent daily mean ± standard deviation obtained from the Brazilian National Institute Meteorological (INMET) station in São Paulo.

| Date | GBGI | Objects | Vehicles | Humans | Miscellaneous | Ambient Temperature |
|---|---|---|---|---|---|---|
| Day 1 | 18.2 ± 4.1 | 26.2 ± 8.7 | 19.0 ± 2.2 | 19.8 ± 4.0 | 18.6 ± 2.9 | 21.9 ± 3.3 |
| Day 2 | 16.6 ± 3.1 | 15.8 ± 3.8 | – | 19.5 ± 4.8 | 14.8 ± 3.4 | 20.2 ± 1.5 |
| Day 3 | 17.2 ± 3.2 | 17.7 ± 0.7 | 17.6 ± 1.0 | 17.8 ± 0.8 | 17.4 ± 4.4 | 20.0 ± 3.2 |
| Day 4 | 21.0 ± 6.2 | 21.4 ± 6.4 | 21.7 ± 7.2 | 20.7 ± 4.2 | 21.7 ± 8.1 | 21.9 ± 2.8 |
| Day 5 | 16.2 ± 0.8 | 16.7 ± 0.7 | 16.7 ± 1.2 | 17.0 ± 0.6 | 16.6 ± 1.1 | 19.0 ± 1.6 |
| Day 6 | 15.7 ± 3.7 | 16.1 ± 3.7 | 13.8 ± 5.2 | 17.5 ± 6.1 | 15.6 ± 4.2 | 19.4 ± 2.7 |
| Day 7 | 15.9 ± 1.7 | 16.6 ± 1.7 | 17.3 ± 0.6 | 17.4 ± 0.7 | 16.4 ± 1.8 | 20.7 ± 2.8 |
| Mean | 17.3 ± 3.3 | 18.6 ± 3.7 | 17.7 ± 2.9 | 18.5 ± 3.0 | 17.3 ± 3.7 | 20.5 ± 2.5 |

morning hours appears to create a stagnant air environment during periods of reduced atmospheric mixing, effectively trapping pollutants generated within or advected into the park [28]. This is particularly relevant for BC, which showed a pronounced midday peak likely associated with increased vehicular traffic along the park perimeter during lunch hours, followed by limited dispersion under dense canopy cover.

The influence of humidity on particulate matter dynamics within the vegetated zones warrants particular attention. A slight afternoon increase in $PM_{2.5}$ within the park (~0.4 μg $m^{-3}$) coincided with elevated relative humidity under dense canopy cover, consistent with hygroscopic particle growth. Under high humidity, aerosols absorb water, increasing optical detectability and altering deposition dynamics, with significant growth reported above 50% RH and up to a five-fold rise in deposition velocity at > 95% RH[91]. Similar behaviour has been documented in tropical coastal settings; for example, biomass-burning aerosols in Singapore exhibit a 2.6-fold increase in light scattering at 90–95% RH due to their high sulfate and water-soluble organic carbon content [92]. Although particle size distributions were not measured directly, the concurrent rise in $PM_{2.5}$ and humidity aligns with hygroscopic growth processes observed in comparable tropical environments.

The magnitude of BC reductions along our transect aligns with expectations for diffuse urban–park interfaces. Roadside studies in Singapore report 20–60% BC reductions behind dense vegetative barriers, depending on configuration[93], values higher than ours due to their focus on immediate roadside–barrier contrasts rather than gradual transitions across heterogeneous canopy structures. These studies also highlight vegetation as an effective deposition surface for particles of diverse morphology[93]. Work from tropical Indian megacities further shows strong meteorological modulation of BC, with coastal wind regimes and shifting fossil-fuel versus biomass-burning sources influencing depletion rates[94]. Together, these findings indicate that vegetation-mediated BC reduction in tropical settings is highly dependent on site configuration, local meteorology, and emission characteristics.

These findings reinforce the concept that urban vegetation serves as a dynamic component of the urban airshed rather than a passive filter [28]. The effectiveness of pollution mitigation depends not only on vegetation density but also on canopy structure, park geometry, and the interplay with local emission patterns and atmospheric conditions. This complexity underscores the need for strategic vegetation management that optimises both filtration capacity and air mixing, particularly in areas prone to traffic-related pollutant influx.

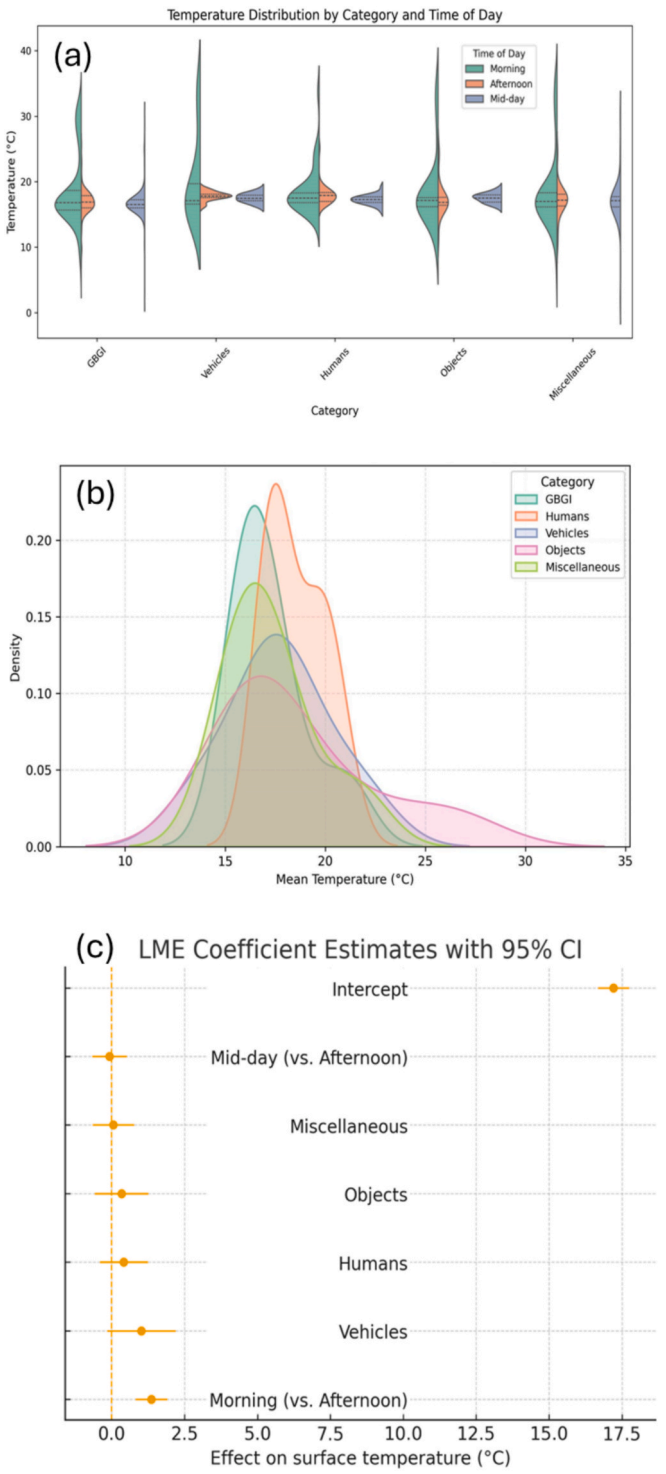


**Fig. 10. (a)** Violin plots of surface temperatures by image category (GBGI, Humans, Vehicles, Objects, Miscellaneous) and time of day (morning, midday and afternoon), illustrating differences in central tendency and spread. Wider sections indicate higher data density. **(b)** Kernel density curves of surface temperatures by category. GBGI peaked narrowly around 17 °C, while Objects showed the widest dispersion. **(c)** Coefficient estimates from the linear mixed-effects model assessing the influence of category and time of day on surface temperatures. Points represent model estimates; horizontal bars show 95% confidence intervals (dashed line = null effect). Full statistical outputs are provided in **SI Table S9**.

### 4.2. Microclimate regulation

The documented temperature and humidity gradients across the urban-park interface exemplify the powerful regulatory capacity of vegetated spaces in moderating urban microclimates. The park's consistent cooling effect, with temperatures 1-2 °C lower than adjacent urban areas during peak heating hours, demonstrates the combined efficacy of shading and evapotranspiration processes that have been widely documented in urban climate literature[95]. This cooling effect was most pronounced during midday and afternoon periods when solar radiation intensity was greatest, highlighting the temporal variability of vegetation's moderating influence. This consistent with Yu et al. [38] showing stronger daytime cooling in humid zones and enhanced nocturnal cooling in arid climates.

The complementary relationship between temperature and RH observed along the transect reveals the fundamental role of plant physiology in microclimate regulation. The elevated RH within the park core (reaching 73.1% at midday) directly results from transpirational cooling, a process where vegetation releases moisture into the atmosphere while converting sensible heat to latent heat[90]. This physiological process explains the inverse correlation between temperature and humidity gradients and underscores how vegetation simultaneously addresses both thermal and moisture aspects of human comfort. The sustained higher humidity in the park during the afternoon (68.4%) compared to the sharp decline at the exposed eastern roadside (63.3%) demonstrates vegetation's capacity to maintain more stable microclimatic conditions throughout diurnal cycles.

The connection between vegetation-driven humidity and carbon dioxide patterns provides insight into the intertwined biogeochemical processes governing urban atmospheres. The stable $CO_2$ concentrations within the park, with only a slight increase from 539 ppm in the morning to 549 ppm in the afternoon, contrast with the elevated $CO_2$ levels in western urban zones (exceeding 556 ppm at midday). This pattern reflects the competing influences of anthropogenic emissions and photosynthetic activity [28].

The observed thermal comfort patterns, particularly the disconnect between air temperature reduction and thermal comfort during midday hours, highlight the complex interplay between physical parameters and human sensation. While the park provided measurable cooling, the elevated humidity partially offset the temperature reduction in terms of human thermal comfort, as reflected in the PET and UTCI indices [95,96]. This illustrates the importance of considering integrated comfort indices rather than individual parameters when evaluating the microclimatic benefits of urban greenery, particularly in warm-humid climates where humidity plays a crucial role in human heat balance.

The midday divergence between reduced air temperature and limited thermal comfort, driven by elevated humidity within the park core, highlights a key design challenge for GBGI in warm-humid climates. Although dense vegetation enhances cooling via evapotranspiration, the accompanying moisture can diminish perceived comfort when airflow is restricted, underscoring the need to balance vegetation density with ventilation [97,98]. Recent work on vegetation–building–meteorology interactions suggests how such balance can be achieved. Studies of vegetated facades show that high-LAI vegetation enhances cooling in well-ventilated areas, whereas in low-ventilation settings, thinner vegetation maintains more stable microclimates by preserving airflow[97]. Applied to parks, this implies that heterogeneous canopy configurations—providing shade while maintaining ventilation corridors, may optimise comfort. Established tropical design guidance similarly emphasises arranging vegetation to provide shading crowns without obstructing wind at pedestrian level [99]. Vegetation cooling efficacy may also vary with plant physiological responses. In tropical savanna climates, canopy cooling declines during peak heat due to reduced evapotranspiration under high vapour-pressure-deficit conditions[100], indicating that species choice and irrigation regimes are important alongside spatial design. Collectively, these insights point

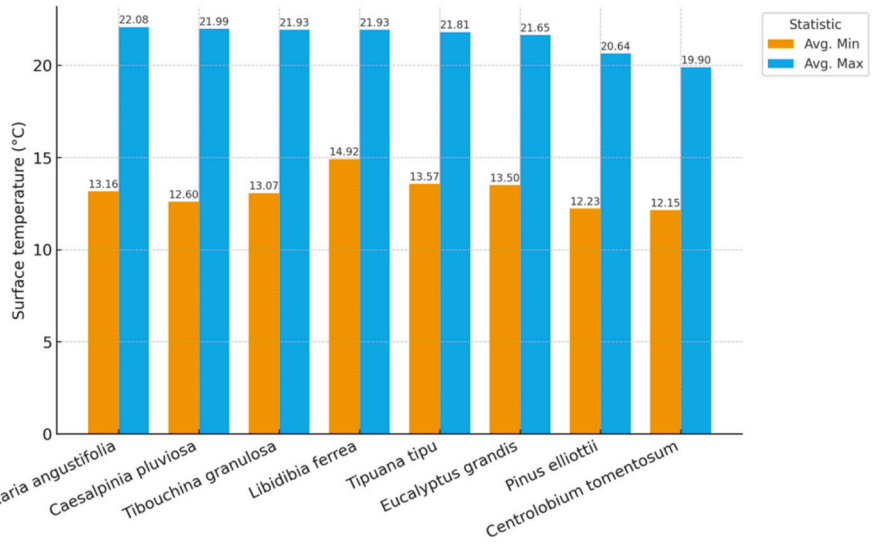


**Fig. 11.** Average minimum and maximum surface temperatures (°C) by tree species. Bars represent values across monitoring points dominated by each species, highlighting differences in cooling capacity related to canopy structure and physiology.

toward park layouts that maximise airflow while retaining shade. Recommended strategies include using tall, high-crown trees that allow ventilation beneath the canopy [98], maintaining wind-aligned ventilation corridors, selectively thinning understory vegetation in high-use areas, and favouring species with open rather than dense ground-to--canopy foliage. Such approaches align with long-standing principles for warm-humid climates, where vegetation should moderate solar loads without impeding prevailing winds[99]. The strong correlation between SVF and thermal comfort indices, particularly the highly significant afternoon relationship ($p < 0.001$; slope = 10.6 for PET), consistent with Zhou et al. [39] findings showing ~ 3.7 °C UTCI cooling in vegetated areas and optimal performance when 3D canopy per tree remains below 22 $m^3$. Together, these studies underscore the joint importance of horizontal cover and vertical foliage structure for urban cooling[96]. The significantly stronger effect of SVF on thermal comfort in the afternoon compared to morning periods illustrates how vegetation's shading function becomes increasingly valuable as heat accumulates throughout the day. This temporal pattern of vegetation's benefit aligns with the concept of cooling efficiency being highest when thermal stress is most severe.

### 4.3. Noise attenuation

The acoustic environment along the urban-park transect demonstrated more complex patterns than the steady attenuation often assumed for vegetated areas. While the general trend of decreasing noise levels from urban edges to the park core was observed, particularly during morning hours (approximately 0.29 dB reduction per 100 m), the appearance of noise peaks within the park itself highlights the multifaceted nature of sound propagation in urban green spaces[101].

The modest but consistent reduction in noise levels from built-up zones to the park core, especially evident during morning measurements, supports the established understanding that vegetation can function as an acoustic buffer through sound absorption and deflection [101]. While a 6 dB reduction may appear modest in absolute terms, it represents a clearly noticeable change in human perception, approximately a halving of perceived loudness [102], and constitutes a meaningful improvement in acoustic comfort for park users. The denser canopies in the park interior likely contributed to this attenuation through a combination of surface absorption and scattering of sound waves. However, the reversal of this gradient in the afternoon, with noise increasing toward the highway, suggests that vegetation's acoustic benefits have limitations against highly dominant noise sources and that diurnal patterns of human activity significantly influence soundscapes.

The presence of localised noise peaks within the park, particularly during midday hours, suggests that internal sound sources (such as recreational activities, pedestrian traffic, or park maintenance) can outweigh the buffering capacity of vegetation, particularly in busy parks with lots of human activity. This observation aligns with research suggesting that while vegetation can moderate continuous background noise, it may be less effective at attenuating discrete, nearby sound sources[101]. The co-location of high NDVI values and lower midday noise levels at the eastern roadside suggests that strategic vegetation placement can enhance acoustic comfort even in predominantly urban zones, though the effect size remains modest compared to source distance and activity patterns.

The observed inverse relationship between NDVI and noise levels during midday hours, while demonstrating a measurable physical attenuation, also aligns with a characteristic of effective vegetative noise barriers. Denser vegetation (high NDVI) not only contributes to sound absorption but also often creates a visual screen that can block the line-of-sight to noise sources. While this study did not measure perceptual responses, the physical association between denser greenery and lower noise levels suggests that the park's vegetation provides acoustic buffering that is both quantifiable and likely to contribute to a more subdued acoustic environment. This underscores that the acoustic benefit of urban parks encompasses a tangible reduction in sound levels, as measured in this study.

### 4.4. Limitations and future research

This study provides valuable insights into the environmental gradients across an urban-park interface, yet several limitations warrant consideration. The transect-based mobile monitoring approach, while capturing fine-scale spatial variations, represents a snapshot under specific meteorological conditions. Future research would benefit from extended monitoring across multiple seasons to capture the effects of phenological changes in vegetation, particularly in deciduous species where leaf area index variations significantly alter shading, transpiration, and filtration capacities[90]. Additionally, while the study documented clear spatial patterns, the mechanistic relationships between specific vegetation structural traits and environmental parameters merit deeper investigation.

The methodological approach of using a first-order polynomial fit to

quantify spatial gradients proved effective for identifying dominant monotonic trends, though not all relationships reached statistical significance. This approach focused on physical interpretation of gradients rather than strict statistical significance, but future studies with larger sample sizes could employ more complex modelling approaches to capture potential non-linear relationships, particularly at the ecotone between urban and vegetated zones.

The temporal patterns observed in environmental parameters reveal important considerations for aligning human activity with environmental benefits. The pronounced afternoon cooling effect (0.2 °C per 100 m gradient), coinciding with the steepest reduction in PET values and the strongest SVF-comfort relationship, suggests that the park's thermal benefits are most substantial during late afternoon hours. This temporal alignment carries significant implications for park management and urban design. Research on park usage patterns demonstrates that thermal comfort is a primary motivator for park visitation on warm days, with visitors actively seeking shaded areas to mitigate heat stress [103]. Studies using smartphone location data have shown that park attendance patterns are strongly influenced by time of day, with visitors adjusting their behaviour in response to thermal conditions[104]. If recreational use peaks during late afternoon hours, as is common in many urban parks following the workday, the maximum environmental benefit would align with maximum human occupancy, potentially enhancing park utilisation and physical activity during periods that were previously limited by thermal discomfort[95,96]. Furthermore, evidence from tropical and subtropical cities indicates that visitors consciously select park locations based on thermal conditions, preferring waterside and densely vegetated areas during peak heat periods [105]. This behavioural adaptation underscores the importance of designing parks that provide targeted cooling where and when people need it most.

Conversely, the complex air quality patterns, including the midday BC peak and occasional $PM_{2.5}$ elevation within the park, suggest that certain park areas might be best utilised during morning hours when air quality improvements are most consistent. This temporal misalignment of benefits (thermal comfort peaking in afternoon, air quality often best in morning) presents both a challenge and opportunity for park management and programming. Staggering activities based on sensitivity to different environmental parameters could optimise the recreational experience while minimising exposure to less favourable conditions. The implications for urban planning and design are substantial. The demonstrated environmental gradients support the value of distributed green infrastructure throughout urban areas, reducing the distance residents must travel to access these benefits [90]. The species-specific performance variations in surface temperature regulation highlight the importance of strategic species selection based on desired ecosystem services, with dense, irregular canopies like *Pinus elliottii* and *Centrolobium tomentosum* showing superior cooling performance compared to more open canopies [90].

Future research should focus on quantifying the exact spatial extent of park influence into surrounding urban areas, particularly for cooling effects which appear to extend beyond park boundaries during afternoon hours. Integrating these environmental measurements with simultaneous social science methodologies capturing human activity patterns and perceptions would provide a more complete understanding of how environmental modifications translate into improved human experiences and health outcomes. Such integrated approaches could optimise green infrastructure investments to maximise multiple ecosystem services aligned with human use patterns, creating more resilient and livable urban environments.

Future research should include multi-seasonal monitoring to assess the year-round GBGI performance, and should integrate biometric data (e.g., heart rate or stress levels) to directly measure how these environmental benefits translate into improved human health. Our monitoring campaign focused on particulate matter ($PM_{2.5}$, BC) and $CO_2$, but did not measure gaseous pollutants such as $O_3$ and nitrogen dioxide ($NO_2$), which exhibit complex and sometimes counterintuitive interactions with vegetation. Recent modelling studies in European cities have demonstrated that vegetation can both reduce and increase $O_3$ concentrations depending on context: while dry deposition removes $O_3$ from the atmosphere, biogenic volatile organic compounds (BVOCs) emitted by vegetation can participate in photochemical reactions that form $O_3$, leading to highly spatially variable effects within urban areas [106]. Similarly, $NO_2$ concentrations may increase locally under dense canopies due to reduced ventilation, despite vegetation's capacity for $NO_2$ uptake through stomatal deposition[107]. The net effect of urban vegetation on these pollutants depends on complex interactions among meteorology, background chemistry, and vegetation characteristics that our study design could not capture. Future research should incorporate $O_3$ and $NO_2$ monitoring alongside particulate measurements to provide a more complete assessment of the multifunctional air quality benefits, and potential trade-offs, of urban green infrastructure in tropical megacities. Advanced remote sensing like LiDAR should be used to quantify vegetation structure more precisely, and the replicable methodology should be applied across diverse urban morphologies to develop tailored, transferable design principles.

## 5. Summary and conclusions

This study provides a high-resolution, spatio-temporal quantification of the environmental benefits generated by Ibirapuera Park, a critical GBGI within the tropical megacity of São Paulo. By integrating mobile transects, stationary monitoring, and thermal imagery, our findings demonstrate that the park functions as a significant environmental regulator, though the efficacy of this regulation is complex, contingent on diurnal timing, vegetation structure, and proximity to anthropogenic sources. The key conclusions drawn are:

- Stationary monitoring showed a distinct edge-to-core gradient, with $PM_{2.5}$ and BC concentrations 31–40% lower in the densely vegetated park interior compared to road-proximal edges. Mobile monitoring corroborated this buffering effect: morning $PM_{2.5}$ and BC declined by 0.07 and 0.03 $\mu g\ m^{-3}$ per 100 m toward the park core, whereas midday $CO_2$ increased by 1.93 ppm per 100 m into built-up areas. Filtration efficiency varied by species, with dense, multi-layered canopies most effective at intercepting particles, particularly during midday when pollution plumes advected inward. The park's role in air quality regulation reflects a dual nature of vegetation. While dense canopy cover consistently filtered pollutants, reducing $PM_{2.5}$ and BC by up to 40%, it also restricted dispersion, causing localised midday peaks within the park. This highlights vegetation as a dynamic component of the urban airshed; its filtration benefits can be partly offset by microclimatic influences on air mixing.
- The park's vegetation produced a strong cooling effect, with core air temperatures consistently 1–2 °C lower than adjacent built-up areas and up to ~ 2.5 °C cooler than the periphery. Mobile monitoring showed an afternoon warming gradient of 0.2 °C per 100 m outward from the core, accompanied by a 0.53% per 100 m decline in relative humidity (RH). Cooling was coupled with higher and more stable RH, driven by shading and evapotranspiration. Areas with low sky view factor (SVF) under dense canopy maintained comfortable conditions (UTCI ≈21.7 °C), while exposed zones reached moderate heat stress (UTCI up to 29.3 °C). The influence of SVF on thermal stress intensified through the day, underscoring the critical role of shade during peak solar radiation. Microclimatic regulation emerged as the park's most consistent ecosystem service: a 1–2 °C cooling effect, strengthening to a 0.2 °C per 100 m gradient in the afternoon, paired with elevated and stabilised RH. However, thermal comfort analysis revealed that physical cooling did not always translate linearly to improved thermal comfort, as higher humidity could partially offset temperature benefits at midday. The growing correlation between SVF and thermal stress indices highlights the

importance of dense canopy shading during periods of peak heat accumulation.

- Acoustic monitoring highlighted the park's role as a noise buffer. Multi-layered vegetation provided measurable attenuation, with interior noise levels averaging $\sim$ 52 dB compared to $>$ 58 dB at entrances and pathways. Mobile data showed that morning noise decreased by 0.29 dB per 100 m toward the core, and afternoon levels dropped by 0.25 dB per 100 m from the urban fringe. While vegetation offered acoustic shielding, its effectiveness was modest and varied diurnally and spatially; it was most pronounced against morning background noise and less effective against dominant afternoon sources such as adjacent highways. Overall, noise reduction was influenced more by distance from sources than by vegetation alone, and was often compromised by internal park activities.
- The study revealed that park benefits are dynamic and spatio-temporally variable. Cooling and pollution dilution peaked at midday but were moderated by wind patterns, with pollution roses identifying inflow vectors from major roads. The effectiveness of GBGI is therefore conditional, requiring strategic design: dense, multi-strata native vegetation, wide buffer zones from emission sources, and continuous canopy cover to extend benefits into the urban matrix. These patterns have direct implications for planning and management. Afternoon cooling aligns with peak thermal stress and recreational use, maximizing comfort, while air quality benefits vary more complexly, suggesting activity scheduling could be optimised to match periods of greatest mitigation. Species selection is critical; dense canopies such as *Pinus elliottii* and *Centrolobium tomentosum* delivered superior cooling. Overall, the findings validate well-designed GBGI as multifunctional infrastructure essential for climate resilience, public health, and livability in tropical megacities.

## 6. Recommendations

This study provides the following recommendations for urban greening strategies in tropical megacities, focusing on structural and design principles:

**Prioritise the creation of deep vegetative cores through structural density**: Planning policies should mandate and protect extensive interior park zones with a minimum width of 250–300 m from major roadways. Our findings show that sites L5 and L6, located at this distance exhibited the most significant reductions in $PM_{2.5}$, BC, temperature, and noise. These benefits are driven primarily by structural complexity and multi-layered vegetation architecture. Larger, contiguous green spaces provide enhanced microclimatic regulation compared to fragmented vegetation[4,28], with optimal cooling efficiency influenced by climatic context. Conservation and expansion efforts should therefore focus on maintaining dense, structurally diverse stands that create a continuous canopy, as this vegetation structure proved most effective for multi-stressor mitigation.

**Implement multi-tiered vegetative buffers along traffic corridors**: To mitigate the pronounced edge effects observed near roadways at sites like L1 and L3, wide vegetative buffers should be installed between high-traffic roads and park perimeters. These buffers should consist of dense, evergreen or densely foliated vegetation with multi-layered canopies that create high aerodynamic roughness, enhancing particle deposition and disrupting pollution plumes.

**Optimise vegetation architecture for multifunctional performance**: Municipal planting programmes should prioritise vegetation structural traits with proven performance metrics rather than focusing solely on ornamental species. This study demonstrates that canopy architecture, including density, layering, and coverage is the primary determinant of ecosystem service provision. Planting strategies should favour combinations of trees and understory vegetation that create low sky view factor (SVF $<$ 0.4) conditions, as these structures consistently delivered superior cooling, pollution filtration, and noise attenuation. A performance-based approach to green infrastructure design should guide public procurement and planting decisions.

**Integrate SVF analysis into zoning and design regulations**: Planners should use SVF mapping, as validated by this study's strong SVF-thermal comfort correlation, to identify thermal vulnerability hotspots (e.g., large paved squares, wide streets with low canopy cover). Regulations should require mandatory shading through canopy cover or built structures in areas with SVF $>$ 0.7, particularly in zones of high pedestrian activity. Furthermore, open areas within parks identified as localised heat spots should be enhanced with strategic tree planting to create continuous canopy cover and uniformly extend thermal benefits.

**Extend park benefits through networked green corridors**: The mobile transect data clearly shows the dramatic environmental transition at the park boundary. Urban design should focus on extending this relief by creating networked green corridors along key pedestrian and cycling routes. These corridors, featuring continuous canopy cover and structural complexity similar to park interiors, would effectively lengthen the 'park experience', protecting residents during daily transit and reducing cumulative exposure to urban stressors.

**Align park design and programming with diurnal benefit patterns to maximise human well-being**: The temporal coincidence between peak afternoon cooling benefits and potential post-work recreational hours suggests that park planning should consider not only spatial configuration but also temporal access. Design strategies should prioritise shading in areas likely to be used during late afternoon periods (e.g., pathways connecting residential areas to park entrances, seating areas oriented to capture afternoon breezes). Park programming, such as outdoor exercise classes, community events, or children's activities, should be scheduled during periods when the park's microclimatic benefits are maximised (late afternoon) rather than midday when thermal stress remains elevated despite cooling. This alignment of human activity with environmental benefit periods can enhance park utilisation, support physical activity, and improve public health outcomes in tropical cities[103,104].

## CRediT authorship contribution statement

**Jeetendra Sahani:** Writing – review & editing, Writing – original draft, Validation, Methodology, Formal analysis, Data curation, Conceptualization. **Akash Biswal:** Writing – review & editing, Writing – original draft, Methodology, Formal analysis. **Anubhav Kumar Dwivedi:** . **Soheila Khalili:** Writing – original draft, Methodology, Formal analysis. **Hao Sun:** Writing – original draft, Methodology, Formal analysis. **Maria de Fatima Andrade:** Writing – original draft, Investigation, Funding acquisition. **Giuliano Maselli Locosselli:** Methodology, Writing – review & editing. **Marco A. Franco:** Writing – original draft, Investigation. **Maria Carla Queiroz Diniz de Oliveira:** Methodology, Writing – review & editing. **Regina Maura de Miranda:** Methodology, Writing – review & editing. **Leticia Figueiredo Candido:** Methodology, Writing – review & editing. **Laurence Jones:** Writing – review & editing, Investigation, Funding acquisition. **Prashant Kumar:** Writing – review & editing, Writing – original draft, Visualization, Supervision, Project administration, Methodology, Funding acquisition, Conceptualization.

## Declaration of competing interest

The authors declare that they have no known competing financial interests or personal relationships that could have appeared to influence the work reported in this paper.

## Acknowledgments

The authors extend their sincere gratitude to the students (Gustavo, Leslie, Caroline, Jorge, Amanda, Rubens, Daniel, Edson, and Ana) from the University of São Paulo (USP) for their invaluable assistance during the extensive field monitoring campaign. This research was generously supported by funding from the NERC-FAPESP funded GreenCities (NE/X002799/1; NE/X002772/1; FAPESP Grant No. 2019/08783-0, 2022/02365-5), the UGPN (University Global Partnership Network) project (UGPN-NBS and GREENICON), GREENIN Micro Network Plus (Grant No. APP55977), GP4Streets (APP44894), and the United Kingdom Research & Innovation (UKRI)-funded RECLAIM Network Plus (EP/W034034/1; EP/W033984/1). The network is jointly funded by three UKRI research councils: the Engineering and Physical Sciences Research Council (EPSRC), the Natural Environment Research Council (NERC), and the Arts and Humanities Research Council (AHRC).

## Appendix A. Supplementary data

Supplementary data to this article can be found online at https://doi.org/10.1016/j.cacint.2026.100360.

## Data availability

Data will be made available on request.

## References

[1] Arnfield AJ. Two decades of urban climate research: a review of turbulence, exchanges of energy and water, and the urban heat island. Int J Climatol 2003;23(1):1–26.
[2] Kumar P, Corada Perez K, Debele SE, Emygdio APM, Abhijith KV, Hassan H, et al. Air pollution abatement from Green-Blue-Grey infrastructure. The Innovation Geoscience 2024;2(4):100100.
[3] Oke TR. The energetic basis of the urban heat island. Q J R Meteorolog Soc 1982;108(455):1–24.
[4] Zhou SQ, Yu ZW, Wu WB, Yang WJ, Zhang YJ, Hao YY, et al. Quantifying cumulative cooling threshold of greenspaces using a newly developed 3D model across global cities. Remote Sens Environ 2025;328:114867.
[5] Ferreira LS, Duarte DHS. Exploring the relationship between urban form, land surface temperature and vegetation indices in a subtropical megacity. Urban Clim 2019;27:105–23.
[6] Gaudereto G, Gallardo A, Ferreira M, Nascimento A, Mantovani W. Evaluation of ecosystem services and management of urban green areas: Promoting healthy and sustainable cities. Ambiente and Sociedade 2018;21:e0120.
[7] Kumar P, Debele SE, Khalili S, Halios CH, Sahani J, Aghamohammadi N, et al. Urban heat mitigation by green and blue infrastructure: Drivers, effectiveness, and future needs. The Innovation 2024;5(2):100588.
[8] Voogt; JA, Oke TR. Thermal remote sensing of urban climates. Remote Sens Environ 2003;86(3):370–84.
[9] Emmanuel R, Krüger EL. Urban heat island and its impact on climate change resilience in a shrinking city: the case of Glasgow, UK. Build Environ 2012;53:137–49.
[10] Sahani J, Kumar P, Debele SE. Assessing demographic and socioeconomic susceptibilities to heatwaves in the Southeastern United Kingdom. Sustain Cities Soc 2024;117:105958.
[11] Heal MR, Kumar P, Harrison RM. Particles, air quality, policy and health. Chem Soc Rev 2012;41:6606–30.
[12] Lyu X, Li K, Guo H, Morawska L, Zhou B, Zeren Y, et al. A synergistic ozone-climate control to address emerging ozone pollution challenges. One Earth 2023;6(8):964–77.
[13] Jacobson MZ. *Atmospheric pollution: history, science, and regulation*. Cambridge University Press; 2002.
[14] Pope III CA, Dockery DW. Health effects of fine particulate air pollution: lines that connect. J Air Waste Manage Assoc 2006;56:709–42.
[15] Kumar P, Morawska L, Martani C, Meyer M, Buonanno G, Biskos G, et al. The rise of low-cost sensing for managing air pollution in cities. Environ Int 2015;75:199–205.
[16] Saldiva PHN, Pope CA, Schwartz J, Dockery DW, Lichtenfels AJFC, Salge JM, et al. Air pollution and mortality in elderly people: a time-series study in São Paulo. Brazil Archives of Environmental Health 1995;50(2):159–63.
[17] Chen S, He P, Yu B, Wei D, Chen Y. The challenge of noise pollution in high-density urban areas: Relationship between 2D/3D urban morphology and noise perception. Build Environ 2024;253:111313.
[18] Jones L, Anderson S, Læssøe J, Banzhaf E, Jensen A, Bird DN, et al. A typology for urban Green Infrastructure to guide multifunctional planning of nature-based solutions. Nature-Based Solutions 2022;2:100041.
[19] Aram F, García EH, Solgi E, Mansournia S. Urban green space cooling effect in cities. Heliyon 2019;5(4):e01339.
[20] Oliveira M, Rizzo L, Drumond A. Characterization of air-quality degradation episodes of $PM_{10}$ in the metropolitan area of São Paulo and their relationship with meteorological conditions. Environments 2020;8:143.
[21] Bowler DE, Buyung-Ali L, Knight TM, Pullin AS. Urban greening to cool towns and cities: a systematic review of the empirical evidence. Landsc Urban Plan 2010;97(3):147–55.
[22] Gago EJ, Roldan J, Pacheco-Torres R, Ordóñez J. The city and urban heat islands: a review of strategies to mitigate adverse effects. Renew Sustain Energy Rev 2013;25:749–58.
[23] Abhijith KV, Kumar P, Gallagher J, McNabola A, Baldauf R, Pilla F, et al. Air pollution abatement performances of green infrastructure in open road and built-up street canyon environments: a review. Atmos Environ 2017;162:71–86.
[24] Jones L, Vieno M, Fitch A, Carnell E, Steadman C, Cryle P, et al. Urban natural capital accounts: developing a novel approach to quantify air pollution removal by vegetation. J Environ Econ Policy 2019;8(4):413–28.
[25] Nowak DJ, Crane DE, Stevens JC. Air pollution removal by urban trees and shrubs in the United States. Urban Forestry and Urban Greening 2006;4(3–4):115–23.
[26] Fletcher DH, Garrett JK, Thomas A, Fitch A, Cryle P, Shilton S, et al. Location, location, location: Modelling of noise mitigation by urban woodland shows the benefit of targeted tree planting in cities. Sustainability 2022;14(12):7079.
[27] Grote R, Samson R, Alonso R, Amorim JH, Cariñanos P, Churkina G, et al. Functional traits of urban trees: Air pollution mitigation potential. Front Ecol Environ 2016;14(10):543–50.
[28] Gunawardena KR, Wells MJ, Kershaw T. Utilising green and bluespace to mitigate urban heat island intensity. Sci Total Environ 2017;584–585:1040–55.
[29] Zölch T, Henze L, Keilholz P, Pauleit S. Regulating urban surface runoff through nature-based solutions – an assessment at the micro-scale. Environ Res 2016;157:135–44.
[30] Akaraci S, Feng X, Suesse T, Jalaludin B, Astell-Burt T. A systematic review and meta-analysis of associations between green and blue spaces and birth outcomes. Int J Environ Res Public Health 2020;17(8):2949.
[31] Bi Y, Ya W, Yang D, Mao J, Wei Q. Urban green spaces and resident health: an empirical analysis from data across 30 provinces in China. Front Public Health 2024;12:1425338.
[32] Connerton P, Nogueira T, Kumar P, de Fatima Andrade M, Ribeiro H. Exploring climate and air pollution mitigating benefits of urban parks in São Paulo through a pollution sensor network. Int J Environ Res Public Health 2025;22(2):306.
[33] Ribeiro AP, Bollmann HA, de Oliveira A, Rakauskas F, Cortese TTP, Rodrigues MSC, et al. The role of tree landscape to reduce effects of urban heat islands: a study in two Brazilian cities. Trees 2023;37:17–30.
[34] Ramon M, Ribeiro AP, Theophilo CYS, Moreira EG, Camargo PB, Pereira CAB, et al. Assessment of four urban forest as environmental indicator of air quality: a study in a Brazilian megacity. Urban Ecosystems 2023;26:197–207.
[35] Correa-Ochoa M, Mejia-Sepulveda J, Saldarriaga-Molina J, Castro-Jiménez C, Aguiar-Gil D. Evaluation of air pollution tolerance index and anticipated performance index of six plant species, in an urban tropical valley: Medellin, Colombia. Environ Sci Pollut Res 2022;29:7952–71.
[36] Locosselli GM, de Camargo EP, Moreira TCL, Todesco E, de Fátima Andrade M, de André CDS, et al. The role of air pollution and climate on the growth of urban trees. Sci Total Environ 2019;666:652–61.
[37] Lima, L. de C., Leder, S. M., Silva, L. B. da, and Souza, E. L. de. (2019). Conforto térmico em espaços abertos no clima quente e úmido: estudo de caso em um parque urbano no Bioma Mata Atlântica. *Ambiente Construído*, 19(2), 109–127.
[38] Yu Z, Li S, Yang W, Chen J, Rahman MA, Wang C, et al. Enhancing climate-driven urban tree cooling with targeted nonclimatic interventions. Environ Sci Technol 2025;59:9082–92.
[39] Zhou SQ, Yu ZW, Ma WY, Yao XH, Xiong JQ, Ma WJ, et al. Vertical canopy structure dominates cooling and thermal comfort of urban pocket parks during hot summer days. Landsc Urban Plan 2025;254:105242.
[40] Lima G, Fonseca-Salazar M, Campo J. Urban growth and loss of green spaces in the metropolitan areas of São Paulo and Mexico City: Effects of land-cover changes on climate and water flow regulation. Urban Ecosystems 2023;26(6):1739–52.
[41] Natureza Urbana (2025) https://naturezaurbana.net/en/projects/ibirapuera-park/ (accessed on 02.09.2025).
[42] North Sydney Council (2026). Planting trees guide. DOI: www.northsydney.nsw.gov.au/trees/planting-trees-guide/3.
[43] Barradas V, Miranda J, Esperón-Rodríguez M, Ballinas M. (Re)designing urban parks to maximize urban heat island mitigation by natural means. Forests 2022;13(7):1143.
[44] Khalili S, Fayaz R, Zolfaghari SA. Analyzing outdoor thermal comfort conditions in a university campus in hot-arid climate: a case study in Birjand. Iran Urban Climate 2022;43:101128.
[45] Lam CKC, Lau KKL. Effect of long-term acclimatization on summer thermal comfort in outdoor spaces: a comparative study between Melbourne and Hong Kong. Int J Biometeorol 2018;62(8):1311–24.
[46] Hagler GS, Yelverton TL, Vedantham R, Hansen AD, Turner JR. Post-processing method to reduce noise while preserving high time resolution in aethalometer real-time black carbon data. Aerosol and Air Quality Research 2011;11(5):539–46.
[47] Carbone A, Coutinho S, Tomerius S, Philippi A. Gestão de áreas verdes no município de São Paulo: Ganhos e limites. Ambiente and Sociedade 2015;18(4):201–20.

[48] Tompkins AM, Casallas A, De Vera MV. Drivers of mesoscale convective aggregation and spatial humidity variability in the tropical western Pacific. npj Clim Atmos Sci 2025;8:69.
[49] Zhang J, Gou Z, Lü Y. Outdoor thermal environments and related planning factors for subtropical urban parks. Indoor Built Environ 2019;30(3):363–74.
[50] Kim J, Lee DK, Brown RD, Kim S, Kim JH, Sung S. The effect of extremely low sky view factor on land surface temperatures in urban residential areas. Sustain Cities Soc 2022;80:103799.
[51] Oke TR. *Boundary layer climates*. Routledge; 1987.
[52] Höppe P. The physiological equivalent temperature–a universal index for the biometeorological assessment of the thermal environment. Int J Biometeorol 1999;43(2):71–5.
[53] Climate adapt (2020). Thermal Comfort Indices—Universal Thermal Climate Index, 1979–2020. The European Climate Adaptation Platform Climate-ADAPT. *The European Commission and the European Environment Agency*. Available online: https://climate-adapt. eea. europa. eu/metadata/indicators/thermal-comfort-indices-universal-thermal-climate-index-1979-2019 (accessed on 21 November 2025).
[54] Tao Z, Zhu X, Xu G, Zou D, Li G. A comparative analysis of Outdoor thermal Comfort indicators Applied in China and other Countries. Sustainability 2023;15:16029.
[55] Lv C, Mittal U, Madaan V, Agrawal P. Vehicle detection and classification using an ensemble of EfficientDet and YOLOv8. PeerJ Comput Sci 2024;10:e2233.
[56] Muften, H.A., Khayeat, A.R.H. (2025). Object Segmentation in Thermal Images Using YOLOv8. In: Thampi, S.M., Chaudhary, V., Pathan, AS.K., Ching Li, K., Krishnaswamy, D. (eds) *Fifth International Conference on Computing and Network Communications* (pp. 467-478). CoCoNet 2023. Lecture Notes in Electrical Engineering, vol 1221. Springer, Singapore.
[57] Kruskal WH, Wallis WA. Use of Ranks in One-Criterion Variance Analysis. J Am Stat Assoc 1952;47(260):583–621.
[58] Dunn OJ. Multiple Comparisons using Rank Sums. Technometrics 1964;6(3):241–52.
[59] Seibert P, Beyrich F, Gryning S-E, Joffre S, Rasmussen A, Tercier P. Review and intercomparison of operational methods for the determination of the mixing height. Atmos Environ 2000;34(7):1001–27.
[60] Velasco E, Roth M. Cities as net sources of $CO_2$: Review of atmospheric $CO_2$ exchange in urban environments measured by eddy covariance technique. Geogr Compass 2010;4(9):1238–59.
[61] Loveday J, Loveday G, Byrne JJ, Ong B-L, Morrison GM. Seasonal and Diurnal Surface Temperatures of Urban Landscape elements. Sustainability 2019;11(19):5280.
[62] de Miranda RM, de Fatima Andrade M, Ribeiro FND, Francisco KJM, Perez-Martinez PJ. Source apportionment of fine particulate matter by positive matrix factorization in the metropolitan area of São Paulo, Brazil. J Clean Prod 2018;202:253–63.
[63] Li W, Pan P, Fang D, Guo C. Effects of Plant Communities in Urban Green Spaces on Microclimate and thermal Comfort. Forests 2025;16(5):799.
[64] Stuhlmacher M, Woods J, Yang L, Sarigai S. How does the composition and configuration of green space influence urban noise?: a systematic literature review. Current Landscape Ecology Reports 2024;9(4):73–87.
[65] Frederickson LB, Russell HS, Raasch S, Zhang Z, Schmidt JA, Johnson MS, et al. Urban vertical air pollution gradient and dynamics investigated with low-cost sensors and large-eddy simulations. Atmos Environ 2024;316:120162.
[66] Wu B, Zhao S, Liu Y, Zhang C. Do meteorological variables impact air quality differently across urbanization gradients? a case study of Kaohsiung, Taiwan. China Heliyon 2025;11(2).
[67] Jha P, Joy MS, Yadav PK, Begam S, Bansal T. Detecting the role of urban green parks in thermal comfort and public health for sustainable urban planning in Delhi. Discover Public Health 2024;21(1):236.
[68] Klemm W, Heusinkveld BG, Lenzholzer S, Jacobs MH, Van Hove B. Psychological and physical impact of urban green spaces on outdoor thermal comfort during summertime in the Netherlands. Build Environ 2015;83:120–8.
[69] Silva T, Matias M, Girotti C, Vasconcelos J, Lopes A. Heat stress mitigation by exploring UTCI hotspots and enhancing thermal comfort through street trees. Theor Appl Climatol 2025;156(3):162.
[70] Huang C, Liu K, Ma T, Xue H, Wang P, Li L. Analysis of the impact mechanisms and driving factors of urban spatial morphology on urban heat islands. Sci Rep 2025;15(1):18589.
[71] Zhang J, Zhang H, Qi R. A study of size threshold for cooling effect in urban parks and their cooling accessibility and equity. Sci Rep 2024;14(1):16176.
[72] Qiu L, Ma H, Yuan H, Chen H. Quantify the shading effects on alleviating human thermal stress across different local climate zones in the Yangtze River Delta. Building and Environment 2025;282:113249.
[73] Krüger EL, Minella FO, Rasia F. Impact of urban geometry on outdoor thermal comfort and air quality from field measurements in Curitiba, Brazil. Build Environ 2011;46:621–34.
[74] Wang R, Liu R, Chen Q, Cheng Q, Du M. Effects of sky view factor on thermal environment in different local climate zoning building scenarios—a case study of Beijing, China. Buildings 2023;13(8):1882.
[75] Briegel F, Makansi O, Brox T, Matzarakis A, Christen A. Modelling long-term thermal comfort conditions in urban environments using a deep convolutional encoder-decoder as a computational shortcut. Urban Clim 2023;47:101359.
[76] Abdallah ASH, Hussein SW, Nayel M. The impact of outdoor shading strategies on student thermal comfort in open spaces between education building. Sustain Cities Soc 2020;58:102124.
[77] Morakinyo TE, Lau KKL, Ren C, Ng E. Performance of Hong Kong's common trees species for outdoor temperature regulation, thermal comfort and energy saving. Build Environ 2018;137:157–70.
[78] Karner AA, Eisinger DS, Niemeier DA. Near-roadway air quality: Synthesizing the findings from real-world data. Environ Sci Tech 2010;44(14):5334–44.
[79] Zhu Y, Hinds WC, Kim S, Sioutas C. Study of ultrafine particles near a major highway with heavy-duty diesel traffic. Atmos Environ 2002;36:4323–35.
[80] Baldauf R. Roadside vegetation design characteristics that can improve local, near-road air quality. Transp Res Part D: Transp Environ 2017;52:354–61.
[81] Nowak DJ, Hirabayashi S, Bodine A, Hoehn R. Tree and forest effects on air quality and human health in the United States. Environ Pollut 2014;193:119–29.
[82] Janhäll S. Review on urban vegetation and particle air pollution – Deposition and dispersion. Atmos Environ 2015;105:130–7.
[83] Chu S, Xu W, Zhang D, Lin J, Liu J, Liu S, et al. Urban blue green spaces and tranquility: a comprehensive review of noise reduction and sensory perception integration. Journal of Asian Architecture and Building Engineering 2025:1–22.
[84] Fang CF, Ling DL. Investigation of the noise reduction provided by tree belts. Landsc Urban Plan 2003;63(4):187–95.
[85] Guo H, Sullivan AP, Campuzano-Jost P, Schroder JC, Lopez-Hilfiker FD, Dibb JE, et al. Fine particle pH and gas–particle phase partitioning of inorganic species in Pasadena, California, during the 2010 CalNex campaign. Atmos Chem Phys 2015;15:11223–41. https://doi.org/10.5194/acp-15-11223-2015.
[86] Seinfeld JH, Pandis SN. Atmospheric Chemistry and Physics: from Air Pollution to climate Change. (3rd ed.). Wiley; 2016.
[87] Bond TC, et al. Bounding the role of black carbon in the climate system: a scientific assessment. J Geophys Res Atmos 2013;118(11):5380–552.
[88] Nowak DJ, Crane DE. Carbon storage and sequestration by urban trees in the USA. Environ Pollut 2002;116(3):381–9.
[89] Shashua-Bar L, Pearlmutter D, Erell E. The influence of trees and grass on outdoor thermal comfort in a hot-arid environment. Int J Climatol 2011;31(10):1498–506.
[90] Al-Hajri S, Al-Ramadan B, Shafiullah M, Rahman SM. Microclimate Performance Analysis of Urban Vegetation: evidence from Hot Humid Middle Eastern Cities. Plants 2025;14(4):521.
[91] Katata G, Kajino M, Matsuda K, Takahashi A, Nakaya K. A numerical study of the effects of aerosol hygroscopic properties to dry deposition on a broad-leaved forest. Atmos Environ 2014;97:501–10.
[92] Lee SY, Gan C, Chew BN. Visibility deterioration and hygroscopic growth of biomass burning aerosols over a tropical coastal city: a case study over Singapore's airport. Atmos Sci Lett 2016;17:624–9.
[93] Tran PT, Kalairasan M, Beshay PF, Qi Y, Ow LF, Govindasamy V, et al. Nature-based solution for mitigation of pedestrians' exposure to airborne particles of traffic origin in a tropical city. Sustain Cities Soc 2022;87:104264.
[94] Vaishya A, Raj SS, Singh A, Sivakumar S, Ojha N, Sharma SK, et al. Black carbon over tropical Indian coast during the COVID-19 lockdown: inconspicuous role of coastal meteorology. Environ Sci Pollut Res 2023;30:44773–81.
[95] Yahia MW, Johansson E, Thorsson S, Lindberg F, Rasmussen MI. Effect of urban design on microclimate and thermal comfort outdoors in warm-humid Dar es Salaam. Tanzania International journal of biometeorology 2018;62(3):373–85.
[96] Zou M, Zhang H. Cooling strategies for thermal comfort in cities: a review of key methods in landscape design. Environ Sci Pollut Res 2021;28(44):62640–50.
[97] Zhao Y, Li R, Niu J, Shi X, Gao N. Impact of vegetated facades on microclimate and outdoor thermal comfort across different building morphologies. Build Environ 2025;113614.
[98] Müller N, Kuttler W, Barlag AB. Counteracting urban climate change: adaptation measures and their effect on thermal comfort. Theoretical and applied climatology 2014;115(1):243–57.
[99] Gut, P., & Ackerknecht, D. (1993). Climate responsive building - Appropriate building construction in tropical and subtropical regions, 3.3 Design for warm-humid zones. SKAT. Gallen, Switzerland.
[100] Arosemena Díaz G, Mora A. Impact of suburban landscape on outdoor thermal comfort in tropical savanna climate. Geol Ecol Landscapes 2025:1–12.
[101] Dzhambov AM, Dimitrova DD. Urban green spaces' effectiveness as a psychological buffer for the negative health impact of noise pollution: a systematic review. Noise and health 2014;16(70):157–65.
[102] Peirce JJ, Vesilind PA, Weiner RF. Noise pollution and control. In: *Environmental pollution and control*. (4th ed.,. Butterworth-Heinemann; 1998. p. 327–49.
[103] Anderson CC, Sophie UJ, Schmidt S. Visitor motivations and design feature use for thermal comfort on hot days in Bochum City Park. Germany Urban Forestry & Urban Greening 2024;102:128564.
[104] Woo B, Fruman S, Escobar R, Gallegos A, Kim J, Salomon J, et al. Smartphone location data show park use patterns in extreme heat (Los Angeles, California, USA). Landsc Urban Plan 2026;265:105499.
[105] Junfeng Z, Nuo W. Study on the relationship between summer microclimate and human thermal comfort in urban waterfront parks–Longzi Lake Park in Zhengzhou city as an example. Landsc Ecol Eng 2025;21:341–56.
[106] Wang Y, Flageul C, Maison A, Carissimo B, Sartelet K. Impact of trees on gas concentrations and condensables in a 2-D street canyon using CFD coupled to chemistry modeling. Environ Pollut 2023;323:121210.
[107] Mircea M, Borge R, Finardi S, Briganti G, Russo F, de la Paz D, et al. The role of vegetation on urban atmosphere of three European cities. Part 2: Evaluation of Vegetation Impact on Air Pollutant Concentrations and Depositions. Forests 2023;14:1255.